



**Politecnico
di Torino**

Wind to ammonia: analysis of a Haber-Bosch process coupled with a hydraulic DOT wind turbine

Sara Bocconi

Company supervisor: Federica Perassi

Company co-supervisor: Sebastian Manigard

Academic supervisor: Andrea Lanzini

POLITECNICO DI TORINO. FACOLTA' DI INGEGNERIA ENERGETICA E NUCLEARE.
MAGISTRALE IN INGEGNERIA ENERGETICA E NUCLEARE
TORINO, ITALIA

March 19, 2024

Abstract

Ammonia is a highly efficient energy vector with an established and flexible infrastructure, an easily mastered storage (either compressed or refrigerated), and transportation, posing a candidate solution to mitigate hydrogen's key drawbacks.

Interest in ammonia has increased as it can not only be used as the energy transfer medium but can be 'cracked' back into hydrogen. Moreover, it can also act as fuel in internal combustion engines, turbines, and electrochemical devices.

Typically, ammonia is produced via the Haber-Bosch process, where hydrogen gas and nitrogen gas are mixed and react thanks to the contribution of a catalyst. This process is currently conducted with the use of fossil fuels.

In this research project, an ammonia stand-alone system powered by a [Delft Offshore Turbine \(DOT\)](#) hydraulic wind turbine is simulated. The [DOT](#) concept of an offshore hydraulic drivetrain coupled with a Pelton turbine and seawater reverse osmosis is integrated with a [Proton Exchange Membrane \(PEM\)](#) electrolyzer for hydrogen production and a [Pressure Swing Adsorber \(PSA\)](#) for nitrogen extraction. Ammonia synthesis occurs in an autothermal Haber-Bosch reactor using a wustite ZA-5 catalyst, enabling operation at milder conditions. A numerical model of the plant is built using Python and compared to models in the literature. The simulation results underscore the necessity of storage for continuous operation, incorporating a water tank, a battery, and a hydrogen tank. Notably, the battery alone proves insufficient for prolonged storage. The importance of the recycle stream in stabilizing ammonia production amidst wind fluctuations and managing plant load is observed. Additionally, the results reveal that no more than one-tenth of the turbines are required for water production, including redundancy, giving further insights for a more complete integration of the components of an ammonia plant with the [DOT](#) turbine.

Keywords: Ammonia, Haber-Bosch, Hydrogen, Power to Gas, Wind Energy.

Acknowledgments

I would like to express my gratitude to my family, my Riccardo, Virginia, and Marco for their unwavering support and for always granting me the freedom to pursue my passions.

I extend my sincere appreciation to Federica, my supervisor, who has always been able to inject me a mix of energy, inspiration and confidence through every meeting. I am grateful also for her friendship. I am also thankful to Sebastian, my co-supervisor, for his timely involvement and valuable contributions.

I am deeply indebted to all the individuals who enriched my experience in Delft. Although I will still leave, I will cherish the memories and the camaraderie shared. Special gratitude goes to my flatmates, whose companionship made even the rainy days less wet and the daily life more spicy. Sneha holds a special place in my heart, surpassing the boundaries of a mere flatmate, giving me her everything (aka expensive laptop) to fulfill my dreams (aka finishing the thesis and wander around Europe).

I am immensely grateful to Paul for his exceptional support and constructive feedback on my thesis. Thanks for motivating me to strive to do my best while keeping me dreaming about the slopes awaiting me out of this flat world.

Lastly, I want to extend my appreciation to my friends from Bologna—Terri, Ari, Chiara, Frecia, and Maddalena. Though physically distant, knowing that you are eating some nutritious meals always brings warmth and comfort. Thank you for always being there.

Thanks

Contents

1	Introduction	9
1.1	The principle of the Delft Offshore Turbine	10
1.2	Research questions	12
2	Green ammonia and wind energy	14
2.1	Haber-Bosch process	16
2.2	Wind energy	17
2.3	Wind to ammonia	18
3	Methodology	19
3.1	Literature Review	19
3.2	Methodology	20
3.2.1	Assumption	20
3.3	Wind to Ammonia Production Plant	21
3.3.1	Catalyst	22
3.4	Hydrogen Production	22
3.5	Nitrogen Production	23
3.6	Sizing	24
4	Numerical Model	25
4.1	DOT turbine block	26
4.1.1	Wind turbine	26
4.1.2	RO	27
4.1.3	Proton Exchange Membrane	28
4.1.4	Pressure Swing Adsorber	28
4.1.5	Nitrogen production consumption	28
4.2	Ammonia production block	28
4.2.1	Compression	29
4.2.2	Heat exchanger	30
4.2.3	Catalyst bed	30
4.3	Power Production and Consumption	31
4.4	Simulation time	32
4.5	Code validation	32
4.6	Sizing	34
4.7	Sensitivity Analysis	36
5	Simulation results of a Wind to ammonia plant without storage	37
5.1	Wind Data	37
5.2	Results	37

6	Simulation results of a Wind to ammonia plant with storage	42
6.1	Electrical Storage	43
6.2	Water Storage	43
6.3	Results without hydrogen storage	43
6.3.1	Storage Control Strategy	44
6.4	Hydrogen Storage	47
6.5	Results with hydrogen storage	49
7	Conclusions and future outlooks	52
7.1	Future recommendations and limitations	53
A		57
A.1	Simulations results	57
	Bibliography	65

List of Figures

1.1	Wind turbine scale-up in dimension and capacity with offshore technology.	10
1.2	MicroDOT set up (DOT B.V.).	11
1.3	DOT 500 set-up. A 500kW wind turbine. A closed oil loop, including an oil pump in the nacelle and an oil motor at the base, transfers the torque to the turbine's base, where the water pump is located. The high-pressure water generates electricity in the Pelton turbine.	12
1.4	Schematic of the DOT500pro project. The turbine shaft drives the High Pressure Pump (HPP) located in the nacelle. The high-pressure line is then divided among the Sea Water Reverse Osmosis (RO), which becomes drinking water, and the Pelton turbine, which produces electricity (DOT B.V.).	13
2.1	Molecule of ammonia[1].	14
2.2	Historical ammonia production by feedstock [2].	15
2.3	Process scheme of Steam Methane Reforming (SMR)-based ammonia synthesis.	16
2.4	Rotor and nacelle located on top of a wind turbine tower[3].	18
3.1	Cheema et al. Haber-Bosch (HB) reactor schematic.	19
3.2	Catalyst bed from Cunan et al.	20
3.3	Plant component and schematic	21
3.4	Electrolyzer schematic. On the left is an Alkaline Water Electrolysis (AWE). On the right is a PEM.	23
3.5	Schematic representation of a Pressure Swing Adsorption (PSA) system. Air enters the bed on the left for adsorption into the Carbon Molecular Sieve. Upon saturation, the regeneration process occurs, releasing the nitrogen-rich stream. The two reactors alternate between adsorption and regeneration phases, ensuring uniform nitrogen production [4].	24
4.1	Approach	26
4.2	Wind production curve	27
4.3	On the left osmosis. On the right reverse osmosis [5].	27
4.5	Energy break down among plant components	35
4.6	Energy breakdown among plants component, excluding the electrolyzer.	35
5.1	Wind speed	38
5.2	Power division among the Pelton and RO per time step.	38
5.3	Consumption of hydraulic energy and production of water from the RO module.	39
5.4	Mass flow rate of produced ammonia and total mass flow of the plant per time step.	39
5.5	Wind to Ammonia. Energy obtained from produced ammonia over harvested wind energy per time step.	40
5.6	Wind power and ammonia production per time step.	40
6.1	Plant schematic with battery, water tank and hydrogen tank included.	42

6.2	On top power distribution between Pelton and RO. On the bottom, the water tank charging/discharging, size $15m^3$.	44
6.3	On top 1000kW battery charging/discharging. On the bottom the mass flow in the plant and the ammonia produced. The battery discharges when the load goes below 20% and charge when $P_{wind} > P_{char}$.	45
6.4	On top battery charging/discharging. On the bottom the mass flow in the plant and the ammonia produced. The battery discharges when the load goes below 20% and charge when State of Charge (SOC) < 1	46
6.5	Storage code implementation.	47
6.6	Results with a 100kg hydrogen tank and 20% minimum load. From top to bottom the total mass flow and ammonia produced in the plant, the battery, and the hydrogen tank.	49
6.7	Wind to Ammonia. Energy obtained from produced ammonia over available wind energy per time step.	50
6.8	Ammonia produced and wind power per times step.	51
6.9	Hydrogen production over time.	51
A.1	Water tank charging/discharging, size $10m^3$.	57
A.2	Water tank charging/discharging, size $20m^3$.	58
A.3	On top battery SOC and charging/discharging power flow. On the bottom the load of the plant and the produced ammonia. The battery discharges when the load goes below 50% of the nominal load.	58
A.4	On top battery charging/discharging. On the bottom the mass flow in the plant and the ammonia produced. The battery is 100kW and discharges when the load goes below 20%.	59
A.5	On top battery charging/discharging. On the bottom the mass flow in the plant and the ammonia produced. The battery discharges when the load goes below 50%.	60
A.6	On top battery charging/discharging. On the bottom the mass flow in the plant and the ammonia produced. The battery discharges when the load goes below 40%.	61
A.7	On top battery charging/discharging. On the bottom the mass flow in the plant and the ammonia produced. The battery discharges when the load goes below 30%.	62
A.8	Results with a 50kg hydrogen tank and 50% minimum load. From top to bottom the total mass flow and ammonia produced in the plant, the battery and the hydrogen tank.	63
A.9	Results with a 100kg hydrogen tank and 50% minimum load. From top to bottom the total mass flow and ammonia produced in the plant, the battery and the hydrogen tank.	64

List of Tables

3.1	Air Separation Unit (ASU) comparison [6]	24
4.1	ZA-5 wustite catalyst parameters	31
4.2	Simulation time: comparison between differential equation solver and vectorial form.	32
4.3	Catalyst bed verification data.	33
4.4	Compressor verification data	34
4.5	Heat-exchange verification data	34
4.6	Cooler and condenser verification input data.	34
4.7	Compressor sensibility analysis	36
4.8	Plant sensibility analysis	36
6.1	Storage input	43

Chapter 1

Introduction

Climate Change is defining issues and challenges of the 21st century[7]. As temperatures further increase, many natural disasters that humanity is already facing, namely severe fires, desertification, sea level rise, and more unpredictable and disruptive weather events, will occur more frequently and destructively[7]. The driving cause behind global warming is [Green House Gases \(GHG\)](#) which trap sun rays and heat, increasing the earth's temperature[8]. Burning fossil fuels, such as coal, oil, and gas, account for over 75% of [GHG](#) emissions [9] and, as stated by the General Secretary of the [United Nations \(UN\)](#) Antonio Guterres, during the last COP28, fossil fuel phase-out is inevitable.

As renewable energy becomes increasingly cost-competitive with fossil fuels [10], the main obstacle to their large-scale implementation is their intermittency, which can lead to reduced grid security and stability [11]. Their dependency on weather conditions makes energy storage a key player in the energy transition, as it allows for storing the surplus of energy that can be used to fulfill the energy demand during periods of insufficient production. [Power to Gas \(PtG\)](#) is a viable option to store surplus renewable energy, thus mitigating the unpredictability of [Renewable Energy Sources \(RES\)](#), buffering power curtailments, and diversifying the mix of energy carriers. As the name suggests, [PtG](#) consists of storing the energy produced, for example, in a wind farm, into gas that can be stored, transported, and used as fuel. A viable candidate for [PtG](#) is hydrogen, thanks to its high energy density of 120-142 MJ/kg and its potential to be produced and consumed with clean emissions. Once fed to a fuel cell, hydrogen generates electrical power, emitting only water vapor and warm air.

Due to energy interests, hydrogen demand in 2050 is expected to grow to 42 million metric tons [12]. However, there are many concerns and challenges regarding its implementation. First of all, its safety, as hydrogen is highly flammable; secondly, the economic viability of its storage and transportation. A high gravimetric energy density characterizes hydrogen, but its volumetric energy density is between 8.49 and 4.5 MJ/L, respectively, in liquid and gaseous states. At atmospheric pressure, 1 kg of hydrogen occupies $12m^3$. Therefore, the attention is shifting to another chemical compound that can carry hydrogen: ammonia. Ammonia is commonly known as the base of fertilizer and is currently produced through the [HB](#) process, traditionally powered by fossil fuels. At the moment, three possible methods are considered for decarbonizing the ammonia production[13]:

- Conventional production with sequestration of the carbon dioxide,
- Hydrogen production via water electrification using renewable energies (wind, solar, and tidal wave, etc.) in a modified small-scale Haber-Bosch (HB) process (eHB),
- Development of alternative methods of production (i.e., electrochemical process)

In this research project, the second method will be discussed. The goal is to design an ammonia production plant powered by a hydraulic transmission wind turbine produced by the Dutch company [DOT](#). The [DOT](#) turbine technology can generate desalinated water and electricity. Building upon this foundation, the company aims to harness these outputs to produce hydrogen through electrolysis. Looking

forward and recognizing the inherent advantages of ammonia over hydrogen in terms of storage and transportation, DOT is already contemplating integrating green ammonia production into its operations. This strategic shift is motivated by recognizing that ammonia offers superior attributes for storage and transport compared to hydrogen. With green ammonia, DOT does not only tap into a more mature and diversified market, but also addresses crucial aspects of logistics and scalability. Consequently, the company is actively evaluating the feasibility of incorporating green ammonia production into its operations, necessitating a comprehensive understanding of factors such as sizing, electricity requirements, and process streams. This research project aims to ascertain the seamless integration of the DOT hydraulic wind turbine technology with the production of green ammonia.

1.1 The principle of the Delft Offshore Turbine

The capacity of offshore wind turbines is constantly increasing and will become Europe's largest sustainable energy source [14]. Last December, the Netherlands achieved an offshore capacity of 4.7 GW in compliance with the Energy Agreement stipulated in 2013. Now, the Dutch government aims to reach approximately 21 GW of installed offshore wind energy capacity by 2031 [14].

As the capacity of offshore wind turbines is constantly increasing, see Figure 1.1, all of its components are forced to scale up, increasing the weight of the nacelle and the support structure. This translates into larger and heavier components, additional required materials, more complicated and expensive installation, and increased capital cost of the wind turbine. DOT aims to reduce the cost of offshore wind energy

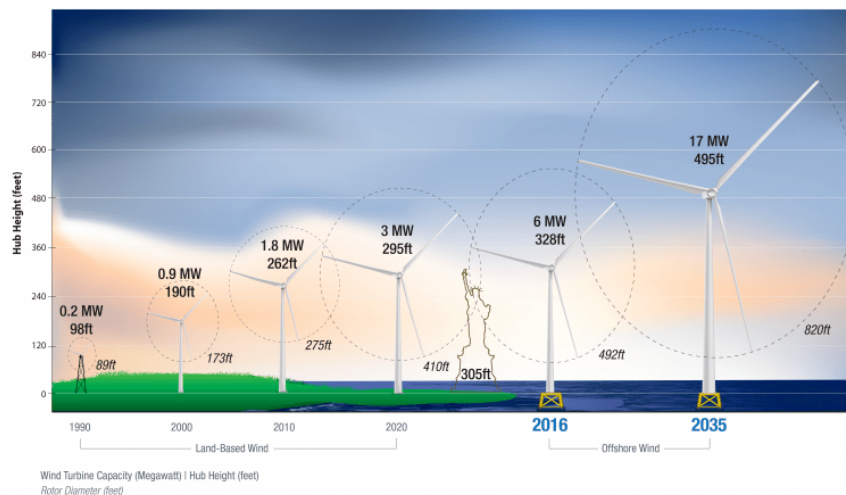


Figure 1.1: Wind turbine scale-up in dimension and capacity with offshore technology.

by tackling these challenges. Lower cost can be achieved with innovative installation methods such as the ones explored in the projects Split Joint, Gentle Driving of Piles (GDP), Hydraulic Pile Extraction Scale Tests (HyPE-ST), and Sustainable Installation of XXL Monopiles (SIMOX)

Their main innovation regards hydraulic power transmission in wind turbines. The first hydraulic power transmission wind turbine was built in 1967. Since then, the concept has been analyzed for its reduced weight, maintenance, and complexity, leading to a lower Levelised Cost Of Energy (LCOE) [15].

DOT's primary technology consists of an open-circuit drive train that uses seawater as a power transmission medium. The rotor shaft of the turbine is directly connected to a HPP, operating at low rotational speed and high torque. With this high-pressure fluid, DOT aims to produce both electricity and desalinated water. To test and evaluate the feasibility of this configuration, the microDOT 10kW project was successfully implemented. The system, shown in Figure 1.2, consists of a small Pelton turbine, an

open-loop freshwater circuit, and a closed-loop hydraulic circuit. From the pump, a high-pressure line leads to a spear valve, where the flow is transformed into high-velocity water jets and converted into electricity through a Pelton turbine [16].

An electric motor operating an oil pump imitated the wind turbine rotor. A nozzle regulating the flow

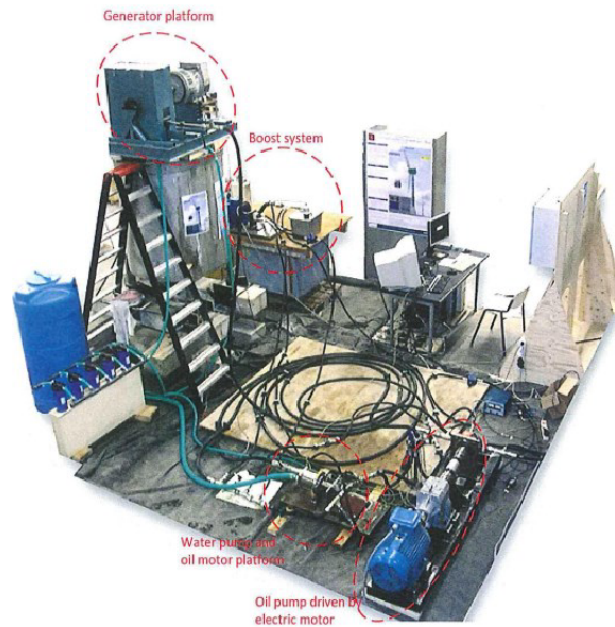


Figure 1.2: MicroDOT set up (DOT B.V.).

towards the Pelton turbine was used to control the system pressure. The prototype scaled up with the [DOT500](#). This set-up consists of a 500 kW hydraulic wind turbine and an oil motor at the tower's base, as shown in [Figure 1.3](#). The oil motor is driven hydraulically by an oil pump connected to the low-speed shaft of the rotor in the nacelle—the closed oil circuit between the rotor and water pump functions as a hydraulic gearbox. The water pump at the bottom of the setup creates a pressurized water flow and is mechanically connected to the motor. The spear valve transforms the flow into high-velocity water jets, and a Pelton turbine-generator setup converts the hydraulic energy into electricity.

With the project [DOT500PRO](#), an RO module is parallel to the Pelton turbine to produce desalinated water.

Parallel to electricity production, that follow the same concept proved with [microDOT](#), an [RO](#) module comprises a variable number of membranes for water production. The pressurized seawater enters the module, which produces permeate (clean water) and brine (a high salt concentration mixture). The system has already been tested with a commercial pump that can produce a flow in the range of 80 to 100 bar. The company has engineered an [HPP](#) capable of generating a water flow at 400 bar, specifically designed to be installed within the turbine nacelle. This innovative design would halve the weight of the nacelle.

The pre-commercial [HPP](#) is undergoing rigorous testing to validate its performance and reliability.

Split Joint is a connection between the wind turbine and its foundation. Generally, wind turbine generators use bolted flange-to-flange connections between the subsequent parts; installing offshore requires multiple lifts. A split joint is based on friction, and the weight ensures a firm and stable connection. Installation is done by simply sliding the wind turbine over the monopile without grout or bolts. This simple mechanism reduces material, equipment, and personnel costs and a shorter installation time [17].

[GDP](#) is a new vibratory installation technology for tubular (mono)piles. It is characterized by the

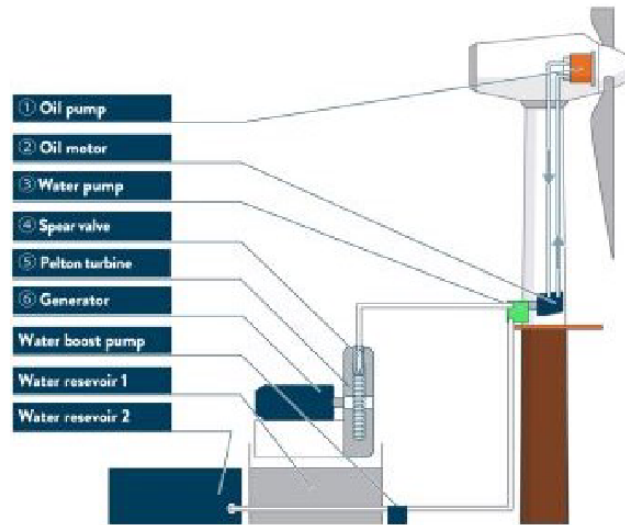


Figure 1.3: DOT 500 set-up. A 500kW wind turbine. A closed oil loop, including an oil pump in the nacelle and an oil motor at the base, transfers the torque to the turbine’s base, where the water pump is located. The high-pressure water generates electricity in the Pelton turbine.

simultaneous application of low-frequency axial and high-frequency torsional vibrations. This method is called “gentle” because of its envisaged capability to reduce the driving loads and the emitted installation noise, which is harmful to the environment [18].

HyPE-ST is a method to remove the entire offshore pile at the end of its life. The technique is based on hydraulic extraction. This method involves sealing the pile after removing the top structure, filling the void with water, and pressurizing it, thus forcing the pile to move upward. This avoids a risky cutting operation underwater and allows the steel obtained to be reused. Hydraulic extraction is expected to be a near-silent method of pile removal. It will, therefore, cause very little disturbance to marine life. No excavation is required for hydraulic pile extraction. The layers of the seabed remain unaffected[19].

The SIMOX project is dedicated to aligning the essential knowledge required for new and innovative installation options. Within this project, the team endeavors to gather the requisite technical and environmental insights, aiming to develop one or more qualified and validated next-generation installation technologies within a timeframe of 5 years.

1.2 Research questions

The project aims to design an ammonia plant powered by a DOT wind turbine and verify its functioning via simulations of a numerical model. Therefore, the following research questions will be answered within the project:

- How would a stand-alone ammonia plant powered by a DOT wind turbine look like?
 - What are the components that constitute a stand-alone ammonia plant?
 - What is the focus on choosing these components?
- How does a Python model compare to the literature simulations, predominantly using Aspen?
 - To quickly and easily assess the performance of the chosen set-up, a simplified numerical model

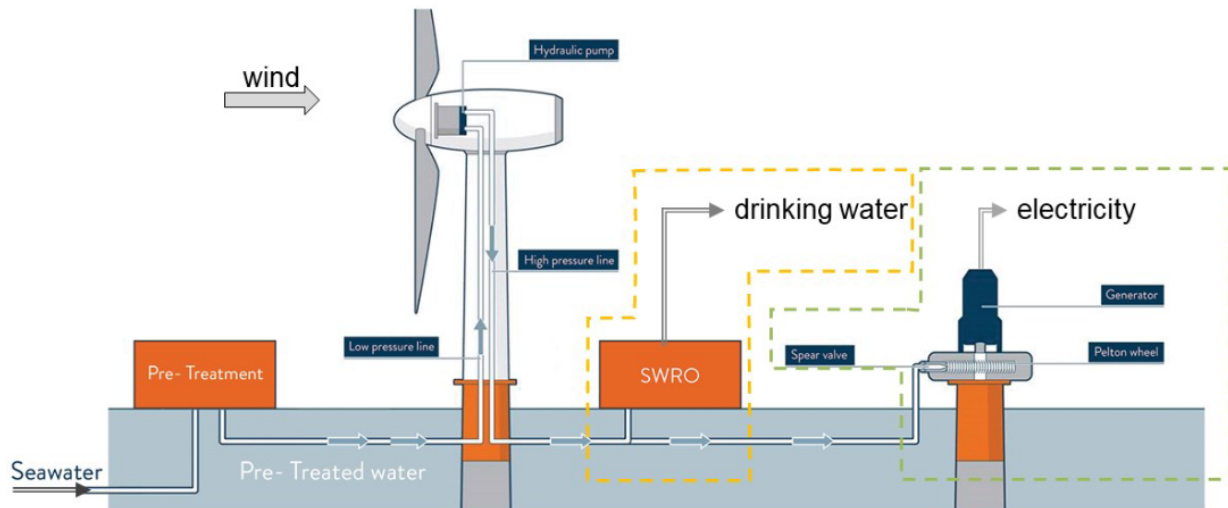


Figure 1.4: Schematic of the DOT500pro project. The turbine shaft drives the HPP located in the nacelle. The high-pressure line is then divided among the Sea Water RO, which becomes drinking water, and the Pelton turbine, which produces electricity (DOT B.V.).

will be created with Python and compared to existing literature. As this consists mainly of models developed on Aspen.

- How will the results obtained with Python differ from the ones in the literature?
- How would such a system operate to keep a relatively steady operation, avoiding starting-up and shutting down sequences?

The plant will have to withstand variable wind conditions; for this reason, a storage system will be added; its goal is to maintain, ideally, quasi-state operation.

- How would storage affect the quasi-state condition?
- How does the minimum load requirement affect the plant operation?

Chapter 2

Green ammonia and wind energy

Ammonia is conventionally known for being the base of fertilizers and refrigerants [20]. However, as the energy transition steps forward, the research on ammonia highlights a new role for its application related to its chemical composition.

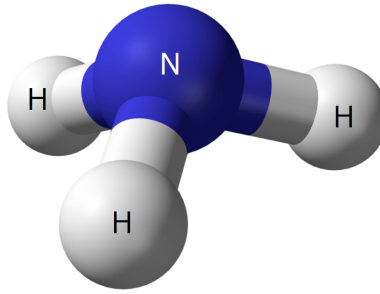


Figure 2.1: Molecule of ammonia[1].

The molecule of ammonia comprises 1 atom of nitrogen and 3 atoms of hydrogen, Figure 2.1, making it an exciting vector for hydrogen transportation. Interest in hydrogen as a clean energy fuel has tripled demand since 1975 [21]. However, its low volumetric energy density raises issues regarding its storage, distribution, and infrastructure, slowing its implementation [12]. On the contrary, ammonia is a relatively efficient energy vector with an established and flexible infrastructure, an easily mastered storage (either compressed or refrigerated), and transportation [22, 2].

Table 2 compares the energy density and volumetric energy of ammonia and hydrogen, both liquid and compressed, with some traditional fossil fuels. Hydrogen stands up among the other substances for its

	$H_2(l)$	$H_2(g)$	$NH_3(l)$	Gasoline	Natural gas	Low-grade coal
MJ/L	8.49	4.5	12.7	32	0.0364	-
MJ/kg	120	120	22.5	44	55	20
T [$^{\circ}C$]	-253	25	-33.4	25	25	25
p [bar]	1	690	1	1	1	1

very high energy density, almost three times that of gasoline. However, its volumetric density is lower than that of ammonia when in liquid and gas. Moreover, both liquefying and pressurizing hydrogen require energy intensive processes.

On the other hand, ammonia presents milder conditions. It condenses at $-33.4^{\circ}C$ at atmospheric pressure, and $25^{\circ}C$ at 10 bar [23], making it logistically easier to store and transport.

Not only can ammonia be cracked down into hydrogen, with an energy density of 22.5 MJ/kg comparable to fossil fuels (20 MJ/kg for low-grade coal and 55 MJ/kg for natural gas) [22], but research and

development are also moving towards using ammonia directly as fuel in internal combustion engines, electrochemical devices, and turbines [24].

Ammonia has a worldwide production of about 174 million tonnes annually [2], making it the second most widely produced chemical commodity [22]. More than 85% of the produced ammonia is used for fertilizers [2]. Its production, which is nowadays almost entirely based on fossil fuels, see Figure 2.2, through the HB process, accounts for around $420 \frac{MtCO_2}{yr}$, which equals to 2% of the annual global GHG emissions [20].

As the world population is projected to increase to over 9 billion in the next 35 years, so is food pro-

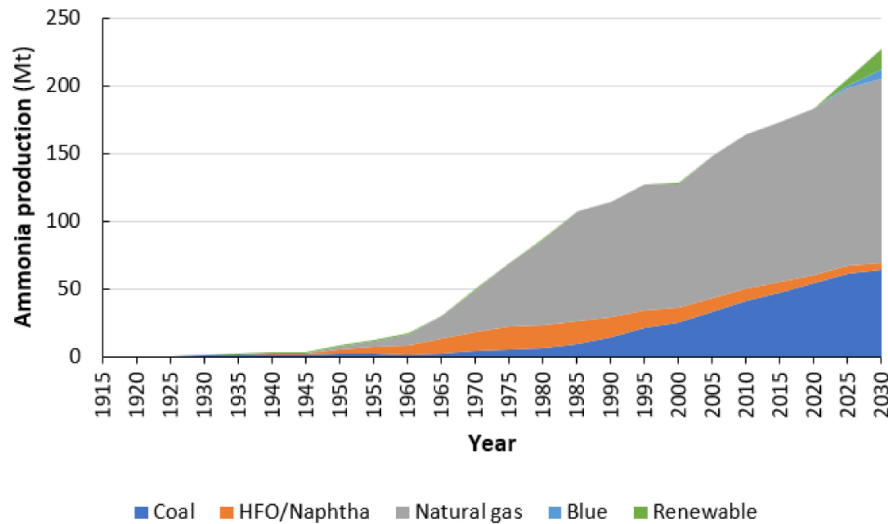


Figure 2.2: Historical ammonia production by feedstock [2].

duction, which in 40%-60% of the cases is dependent on using fertilizers [22, 25], further pushing the ammonia-related GHG emissions.

Furthermore, using NH_3 as a renewable fuel and energy storage mode is expected to increase its demand. Making ammonia production fossil-free would mean reducing agriculture's dependency on fossil fuels and enabling a different vector for the energy transition. Technology enabling the small- and medium-scale synthesis of ammonia can move the production of the fuels closer to the consumer, and - if renewable sources are used - the fuels can be produced carbon-neutral.

Ammonia comes with drawbacks. First of all, ammonia is irritant, corrosive, and may be harmful by all routes of exposure [26]. In many countries, it is classified as a highly hazardous substance and is subject to strict reporting requirements by facilities that produce, store, or use it in significant quantities [27].

Its production is more energy-intensive than hydrogen, as it involves an additional conversion step, as hydrogen needs to be produced first. Moreover, if it is used as a hydrogen carrier and not as an end-fuel, energy is needed to convert it back into hydrogen. Ammonia decomposition is an endothermic reaction that requires high temperatures and low pressures. The temperature ranges from higher than 773 K without the requirement for a catalyst, to lower than 698 K (425 °C)[28]. It is calculated that 1 kg of ammonia would produce 0.18 kg of hydrogen, equivalent to 19.205 MJ of energy. However, approximately 15% of this energy is required for the cracking/processing operation for a net energy production of 16.626 MJ [29]. All these processes and transformations make ammonia production less efficient than hydrogen. If it is directly used as a fuel, it can affect air and water quality due to ammonia leakages and emissions of nitrogen oxides NO_x [30].

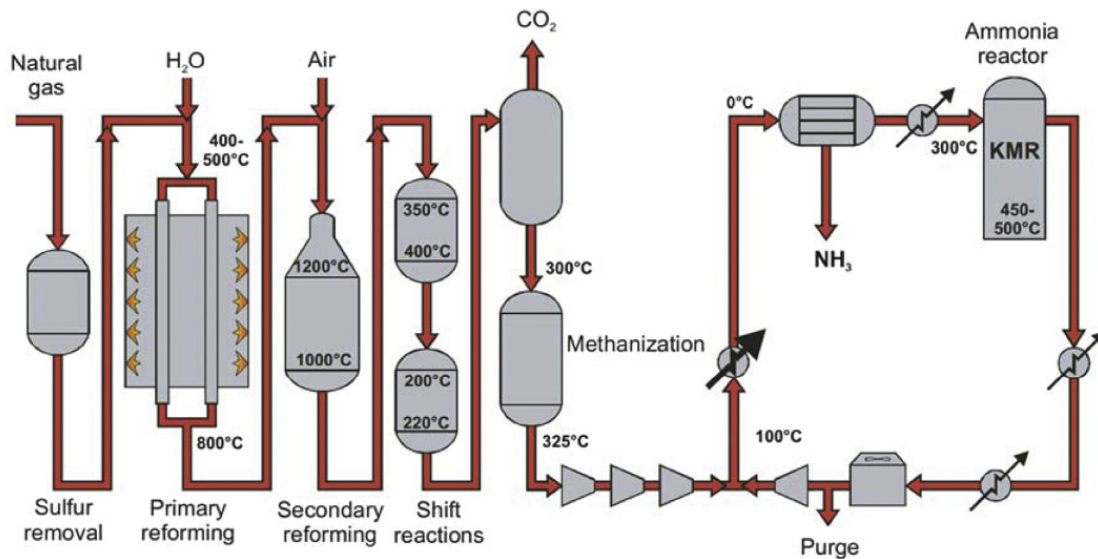


Figure 2.3: Process scheme of SMR-based ammonia synthesis.

2.1 Haber-Bosch process

Ammonia has been synthesized for the last 100 years with the HB process as a result of the work of Fritz Haber and Carl Bosch between 1908 and 1911 [31].

The Haber-Bosch Unit (HBU) unit consists of different components in the HB process.

Nowadays, SMR-based ammonia synthesis, shown in Figure 2.3, is the traditional choice for industrial ammonia production as it is the cheapest and most mature method for large-scale ammonia production. SMR is a chemical process in which methane from natural gas is heated with steam, usually with a catalyst, to produce a mixture of carbon monoxide and hydrogen:



Nitrogen is obtained from air with another reforming process. The carbon oxide is discarded, leaving a nitrogen and hydrogen mixture to be fed into the ammonia synthesis loop. The synthesis of ammonia takes place at high pressure and temperature, conventionally 100-300 bar and 400 – 600°C. Therefore, the mixture’s pressure and temperature are increased by employing a feed compressor and a heater. Once at high pressure and temperature, the nitrogen-hydrogen mix enters the reactor bed, where the synthesis of ammonia takes place:



A catalyst is used to foster the reaction. The choice of catalyst will determine the operating condition of pressure and temperature of the reactor bed, which will be further explained in Subsection 3.3.1.

Once reacted, the mixture is cooled to ammonia condensation temperature, between $-20^\circ C$ and $-30^\circ C$. In the separator, the final product is isolated, ideally pure ammonia.

This separation process leaves a mixture of primarily non-reacted hydrogen and nitrogen. Indeed, a single pass conversion of 20-30% in a bed is typically achieved [32], meaning that most reactants do not react. Therefore, multiple beds are added in succession, and a recycle stream is included to improve the system’s efficiency. The non-reacted hydrogen and nitrogen are compressed back to the loop condition in a recycle compressor, as their pressure is expected to drop due to losses encountered in the loop. The recycle stream is mixed with the new feed of nitrogen and hydrogen coming from the SMR.

Around 5% of the recycle stream is purged to avoid inert gas concentration, namely argon from air [33]. The overall plant conversion, including the recycle stream, is typically 97-99% [6].

To make the production sustainable, fossil fuels must be eliminated from the process in terms of resources (chemical feedstock) and energy sources. Alternatively to methane, hydrogen can be produced from water via electrolysis, and renewable energy sources can power electrolysis and other components. This research aims to show the viability of an [HBU](#) powered by wind energy.

The wind energy harvested by the turbine is transformed through the pump into pressurized seawater. This hydraulic energy is primarily converted into electricity in the Pelton turbine, which will sustain the components of the [HBU](#) and a part of the hydraulic energy is transformed into desalinated water.

2.2 Wind energy

Wind produces electricity by converting the kinetic energy of air in motion into electricity. Global installed wind generation capacity (onshore and offshore) has increased by 98% in the past two decades, jumping from 7.5 GW in 1997 to 733 GW in 2023 [\[34\]](#).

The available energy in the wind is kinetic energy, which is calculated as:

$$E = \frac{1}{2}mU^2 \quad (2.3)$$

Where m is the air mass, and U is the wind velocity. Considering power instead of energy and a mass of wind moving at constant speed:

$$P = \frac{dE}{dt} = \frac{1}{2} \frac{dm}{dt} U^2 = \frac{1}{2} \dot{m} U^2 \quad (2.4)$$

Where \dot{m} is the mass flow rate of air, this can be defined as:

$$\dot{m} = \rho AU = \rho \pi R^2 U \quad (2.5)$$

Where A is the area of the turbine rotor, R the radius of the turbine, U the speed of air. As a result, the power contained in a moving mass flow of air is given by Equation [2.5](#).

$$P = \frac{1}{2} \rho \pi R^2 U^3 \quad (2.6)$$

However, a wind turbine cannot extract all the kinetic power contained in the wind, which would mean that the wind speed is equal to 0 after the turbine. The power extracted is thus only a fraction of the entire kinetic power. The power coefficient c_p , an adimensional parameter, expresses this fraction. The power coefficient represents the ratio of power extracted by the wind turbine relative to the energy available in the wind stream, as reported in the following Equation [2.7](#) [\[35\]](#).

$$c_p = \frac{P_t}{\frac{1}{2} \rho \pi R^2 U^3} \quad (2.7)$$

According to the Betz limit, the maximum power that can be extracted from the wind equals 59.3%. In practice, turbines can achieve up to 75–80% of the Betz limit [\[36\]](#). The power harvested from the wind by a turbine is given by the following Equation [4.5](#), where ρ is the density of air, R is the radius of the turbine, and U is the velocity of the wind.

$$P_{wind} = \frac{1}{2} \pi \rho c_p R^2 U^3 \quad (2.8)$$

There are two traditional types of wind turbines: the [Horizontal-Axis Wind Turbines \(HAWTs\)](#) and [Vertical-Axis Wind Turbines \(VAWTs\)](#). [HAWTs](#) are the most common type of wind turbine [\[37\]](#), usually with three-bladed rotors [\[38\]](#).

A horizontal-axis wind turbine comprises a vertical tower, a rotor, and a nacelle. Both the rotor and nacelle are located on top of the tower. The nacelle is a large, box-like structure, see Figure [2.4](#). It

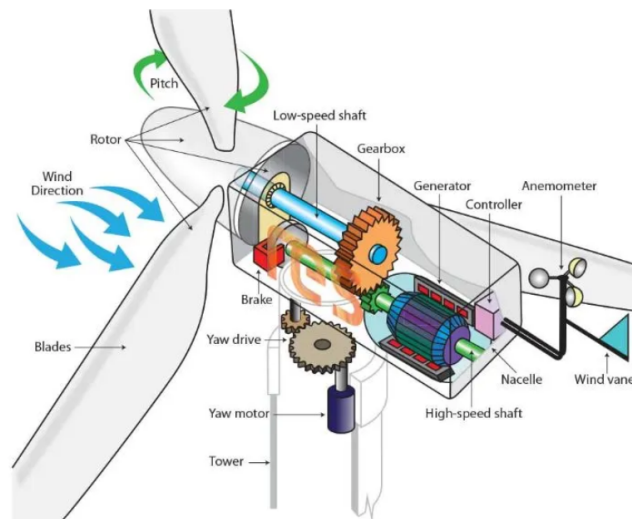


Figure 2.4: Rotor and nacelle located on top of a wind turbine tower[3].

houses many essential elements of the turbine’s operation, including the generator and the gearbox. The rotor is the assembly consisting of the blades and the hub to which they are attached, see Figure 2.4. When the blades rotate, they turn the rotor connected to the low-speed shaft. The low-speed shaft could directly drive the generator in a direct drive configuration [39]. However, the most mature technology uses a gearbox to increase the rotation of the low-speed shaft from 10/20 **Revolution per Minute (rpm)** to 1200-1800 **rpm** on a high-speed shaft. The high-speed shaft is connected to the generator.

2.3 Wind to ammonia

Production of ammonia from renewable sources has gained considerable momentum. The focus is on lowering the operating temperature and pressure condition. Since the end of 2016, REFUEL has been financing projects that aim to produce ammonia from renewable sources and use ammonia as a fuel for electricity generation and transportation [40]. Inside this project, the University of Minnesota is leading a partnership with the U.S. Department of Energy’s National Renewable Energy Laboratory (NREL) and Proton OnSite to develop a smallscale ammonia synthesis system using water and air powered by wind energy and using an innovative absorption separation system to isolate ammonia, which allows for a lower pressure [41].

Siemens has just completed a wind-to-ammonia pilot plant in the United Kingdom and has recently partnered on a larger plant in the Netherlands [42].

At the beginning of 2023, H2Carrier and Greenland-based wind project developer Anori agreed to develop Greenland’s first commercial wind farm, which will power an offshore ammonia production of 900,000 tonnes annually [43].

The proliferation of ongoing projects underscores the profound interest in green ammonia production.

Chapter 3

Methodology

The following chapter provides an overview of the existing literature on ammonia production, particularly from renewable energy sources, and the modeling methods. After that, the methodology of the project is explained.

3.1 Literature Review

Lin et al.[44] compared two configurations for small-scale ammonia production plants: a traditional high-pressure reaction-condensation plant and a more innovative low-pressure reaction-absorption plant. They performed simulations with Aspen Plus and Aspen Custom Modeler, and the results obtained were then used to estimate the total capital and operating costs. The results confirmed that a high-pressure **HB** reaches higher conversions in the catalyst bed; however, lower pressure is beneficial for reducing cost and energy consumption. Cheema et al.[45] focused on the flexibility of the ammonia reactor by analyzing the operating envelope for the steady-state operation of a three-bed autothermic **HBU**, as shown in Figure 3.1. A numerical model of an **HB** reactor was built using MATLAB. The study concluded that the autothermic reactor is viable for the power-to-ammonia process, as it can be operated for a wide range of process variables while maintaining operational hydrogen feed intake and ammonia production flexibilities. Among the six process variables, the H_2/N_2 ratio and inert gas concentration in the reactor system feed provide the most flexibility, up to a ca. 67% decrease in H2 intake.

Verleysen et al. [33] investigate the sensitivity of the ammonia reactor during dynamic operation.

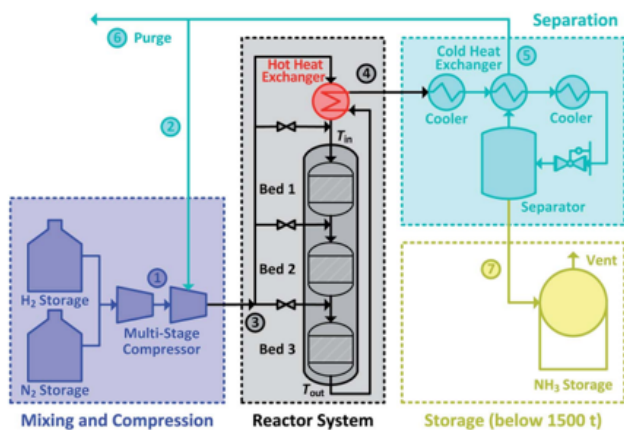


Figure 3.1: Cheema et al. **HB** reactor schematic.

A global sensitivity analysis is performed during ramping-up. The results were that the H_2/N_2 ratio dominates the ammonia production at the start of the ramp-up, where the inlet temperature begins to

dominate the process during the plants' ramp-up.

Cunanan et al.[46] designed and analyzed an on-land small-scale power-to-ammonia production system with a target nominal output of 15 tonnes of ammonia per day, powered by an 8 MW offshore turbine system and an electricity grid as backup. The LCOE of the plant was calculated using Aspen Plus for energy consumption. The ammonia synthesis occurs in 2 catalyst beds, as shown in Figure 3.2.

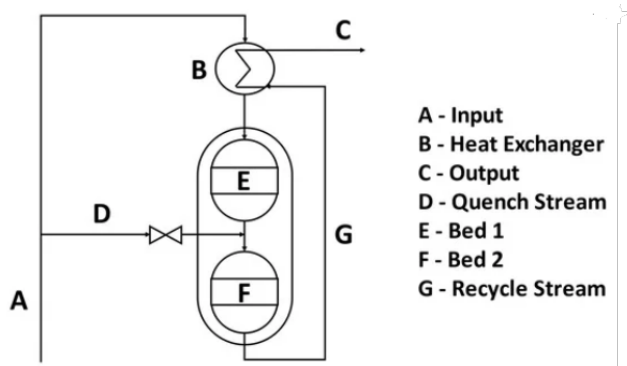


Figure 3.2: Catalyst bed from Cunanan et al.

3.2 Methodology

Previous literature has shown the production process's flexibility, evaluated the plant's capital cost and LCOE of ammonia, and presented the implementation of innovative solutions that allow the plant to operate in less energy-intensive conditions. This research does not consider the economic viability of ammonia and relies on mature technologies that are currently commercially available, thus with a Technology Readiness Level (TRL)>8. The components for the plants are chosen based on their flexibility and energy consumption. Flexibility, the ability to change load, is essential to withstanding unpredictable energy supply. The goal is to maximize ammonia production, thus maximizing electricity utilization to maintain the reactor's stable operation. This means that ammonia production should continue during short periods without wind; storage will be implemented for this purpose. The system is stand-alone, meaning electricity and reactants must be entirely produced on-site. While common practice from the literature was found to be mostly modeling in Aspen, this thesis will model the system components and their interaction in Python. The software will build a numerical model simulating an operational ammonia plant. Using Python and creating a numerical model allows us to simplify calculations and predict the plant's performance over a long period. The plant will be modeled in easily accessible, understandable, and modifiable building blocks. This also allows for further implementation of future works.

Contrary to Aspen, Python is an open-source programming language and does not require any license. To evaluate the proposed ammonia plant, the ammonia production is simulated with a wind data set available from previous research on DOTPRO by [16], and it consists of an average of over 10 years of hourly wind data. The simulation will be performed over one week. After analyzing the initial results, storage will be implemented as a water tank for desalinated water and a battery for electricity. The simulation is repeated with the extended plant, and conclusions regarding the necessity of storage facilities are drawn.

3.2.1 Assumption

The plant model is based on the following assumption:

1. The hydrogen produced from water electrolysis is considered pure.

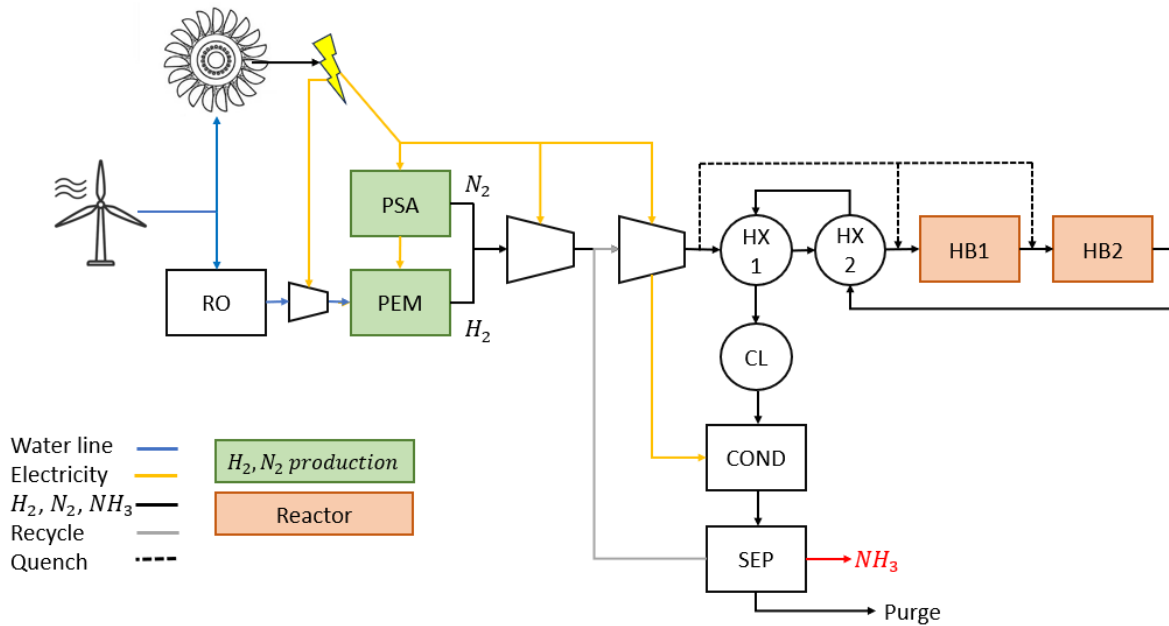


Figure 3.3: Plant component and schematic

2. The production of nitrogen from air neglects argon and other gases.
3. The numerical model only considers the dynamic (part of the) catalyst bed. Other components are considered to handle efficiently the variation of load.
4. The storage of ammonia is not included.
5. The turning on and initial ramping up of the reactor are not considered.
6. The ammonia plant's steady state is assumed to be reached at every time step.
7. Frictional pressure loss in the synthesis loop is assumed to be constant at 3 bar [44].

3.3 Wind to Ammonia Production Plant

Figure 3.3 presents a schematic overview of the system components, including the HBU and the DOT technology components.

Starting from the left side, the wind turbine generates pressurized water via HPP in the nacelle. The water is split between the Pelton and the RO to create electricity and desalinated water. Water enters the electrolyzer, as described in Section 3.4. Electricity is divided among the energy-consuming components, these are electrolyzer (PEM), ASU (PSA), compressors, and condenser, as shown in yellow. The mixture of hydrogen and nitrogen enters a two-stage compressor. The gases are compressed to the operating pressure minus the pressure losses expected over the plant $85-3=82$ bar in the first stage. The feed gas can then be mixed with the recycle stream at a pressure of 82 bar, assuming a 3 bar pressure loss along the circuit. In the second stage, the mixture is compressed to the operating pressure of 85 bar. The mix of gases, heated up due to the compression, is split into 3 streams: a mainstream and two quenching streams added to the main one later on the cycle. This is done for multiple reasons. Firstly, dealing with a smaller stream requires a smaller bed. Secondly, as the reaction is exothermic, the cooling down effect caused by the mixing with the quenching shifts the equilibrium of the reaction

towards ammonia. Thirdly, the in-between bed quench stream decreases ammonia concentration, which also shifts the equilibrium of the reaction towards ammonia[47]. Lastly, this allows for possibly adding temperature control by regulating the quenching fraction. The mainstream is further heated up in two heat exchangers, "HX1" and "HX2", which recover the heat generated by the exothermic reaction in the HBU. Thus, the heat is transferred from the reacted gases exiting the reactor in the previous cycle to the stream entering the reactor. This type of configuration is called an autothermal reaction, meaning that the process is self-sustained by the heat that it produces. This reduces energy consumption, as conventional industrial plants often include an external heater.

After being heated to around 500K-600K, the stream is mixed with the first quench stream and enters the second catalyst bed. As mentioned before, a multi-bed configuration is always beneficial for the presence of the quenching stream. Usually, the number of beds is chosen between 2 and 3. This configuration is selected as it is the same one used by Cunanan et al.[46]. Nevertheless, the catalyst used is the same. The reacted mixture is mixed between the beds with the second quenching stream. Similarly to the industrial plant described in Section 2.1, the reacted mixture is cooled down, first in the two heat exchangers 3.3, then in a cooler "cl", ideally using seawater, and lastly in the condenser. The only energy consumed is in the cooler for pumping seawater and in the condenser, where the temperature decreases to 253K. Finally, the product, the recycle stream, and the purge streams are obtained in the separator.

3.3.1 Catalyst

A catalyst is necessary to overcome the unreactivity of nitrogen. The catalyst must bind to the nitrogen gas. This allows hydrogen to add across the nitrogen bonds until the nitrogen fully saturates, yielding ammonia. Without this crucial catalyst binding, nitrogen remains inert, producing virtually no ammonia. Another factor that contributes to higher reactivity is pressure. Higher pressures indicate more molecular collisions, which increases the reaction rate [47].

The catalyst's choice determines the reactor's operating temperature and pressure [6]. For over 80 years, the HB process has been performed mainly with iron oxide, mostly magnetite, Fe_3O_4 , promoted with potassium and alumina [48], operating at high pressure and temperature at 100/300 bar and 400/500°C [49].

Other potential catalysts exist, including those based on iron. Within this category, specific catalysts utilize wüstite, $Fe_{1-x}O$. Compared to magnetite-based catalysts, wüstite-based catalysts have a lower reduction temperature and less hydrogen inhibition at low temperatures [6].

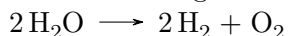
Among the non-iron-based catalysts, Ruthenium-based catalysts stand as highly active. On the downside, this catalyst is relatively more expensive and is easily poisoned by carbon deposition from CH_4 decomposition into syngas ($CO + H_2$). For these reasons, they have found limited uses in conventional HB processes. However, as hydrogen is produced from water and not derived from methane, the poisoning risk does not stand, making Ru a potential candidate for green ammonia synthesis [13].

Introducing wüstite and Ru-based catalysts enables lowering temperature and pressure to the milder conditions at 380°C and 86 bar [46].

For the process to be less energy-intensive, milder conditions are preferred, and a wüstite-based catalyst was selected for this thesis.

3.4 Hydrogen Production

Hydrogen can be produced via various processes; this thesis will focus on electrolysis, which allows the production of H_2 via electricity. In the electrolysis cell, water is split into hydrogen and oxygen according to the following chemical reaction:



As visualized in Figure 3.4, the electrolysis cell comprises two electrodes, a cathode and anode, and a

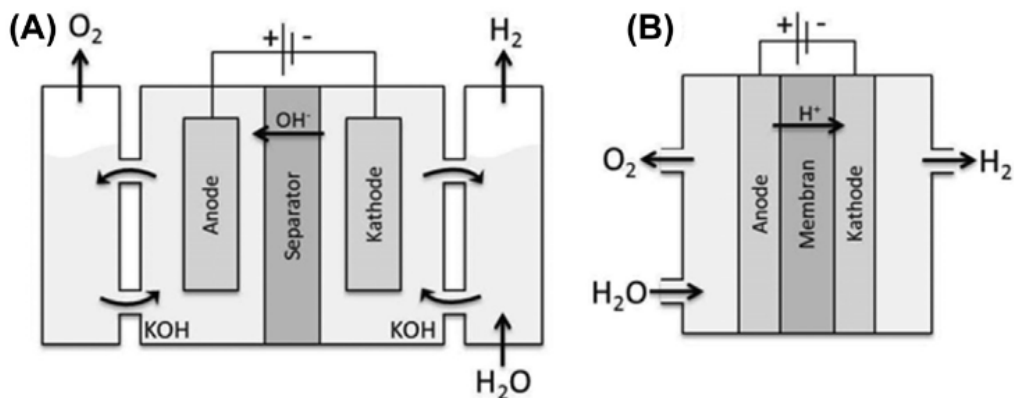


Figure 3.4: Electrolyzer schematic. On the left is an **AWE**. On the right is a **PEM**.

membrane. Electricity, in the form of **Direct Current (DC)**, is applied to the two electrodes, leading to oxidation **Oxygen Evolution Reaction (OER)** at the anode and reduction **Hydrogen Evolution Reaction (HER)** at the cathode, where hydrogen is produced [50] [51].

AWE is currently the most mature electrolysis technology for hydrogen production. It is characterized by the use of alkaline liquid electrolytes[52], typically KOH and NaOH, corrosive substances that require the addition of other materials to avoid damaging the electrodes, decrementing the catalytic activity, and incrementing the operating cost of the process[51].

A less mature technology increasingly entering the market is the **PEM** electrolyzer. **PEM** uses a polymer membrane to transfer protons and works in an acidic electrolyte solution[52].

As shown in Figure 3.4, electrodes are directly coated on the membrane and put into a **Membrane Electrodes Assembly (MEA)**, making it a more compact solution than **AWE**. The use of noble metal for the electrodes leads to high capital costs, one of the major drawbacks of this electrolyzer. The cost can be reduced using different materials, such as mixed oxides of metals from the platinum group, such as iridium and ruthenium[51], and nanostructured thin films[53].

PEM is characterized by high flexibility from 0-5% to 160% [46, 6], a minimum load requirement of 5-10% [46] and fast dynamics (milliseconds scale) [51].

PEM has been chosen over alkaline devices for hydrogen production due to its high flexibility and low minimum load requirement. These characteristics are essential for matching the variability of the renewable output and avoiding dangerous, unstable dynamic effects. Nevertheless, **PEM** can operate at lower cell voltages, higher current densities, higher temperatures, and pressures, leading to higher efficiencies (80–90%)[54, 51]. Since **PEM** can work at a pressure ranging between 30 and 200 bar[55] [6], we assume our electrolyzer will work at 30 bar, and the water entering the system will be pressurized up to this value.

Solid Oxide Electrolysis (SOEC) has yet to be considered as an option as it is still in the laboratory stage. Moreover, its operation at a high temperature of 800°C [53] constitutes a challenging condition for its implementation in a system powered by renewable energy sources.

3.5 Nitrogen Production

Three **ASU** possibilities are considered for nitrogen production: cryogenic distillation, **PSA** and membrane permeation. The choice of technology mainly depends on the scale of the applications and energy consumption, but the grade of purity changes based on the technology[6].

In Table 3.1, the main characteristic of the three **ASUs** are reported: The presented ammonia plant utilizes a **PSA**, which is chosen for its higher operational flexibility compared to other options[56].

	PSA	Cryogenic	Membrane
$T^{\circ}[C]$	-195/-170	20-35	40-60
p [bar]	1-10	6-10	6-25
Purity [%]	99.999	99.8	99.5
Capacity range [Nm^3/h]	250-50000	25-3000	3-30000
Load range [%]	60-100	30-100	
TRL	9	9	8-9

Table 3.1: ASU comparison [6]

The PSA process is based on the phenomenon that under high pressure, gases tend to be trapped onto solid surfaces to be "adsorbed." When pressure is dropped, the gas is released or desorbed, as shown in Figure 3.5. PSA uses the ability of some materials, such as zeolites and activated carbon, to selectively

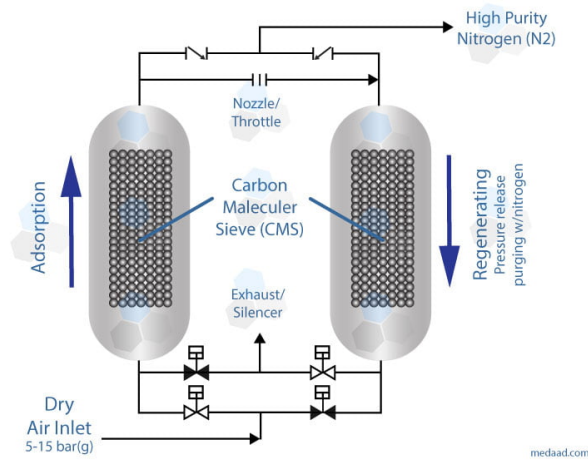


Figure 3.5: Schematic representation of a Pressure Swing Adsorption (PSA) system. Air enters the bed on the left for adsorption into the Carbon Molecular Sieve. Upon saturation, the regeneration process occurs, releasing the nitrogen-rich stream. The two reactors alternate between adsorption and regeneration phases, ensuring uniform nitrogen production [4].

adsorb nitrogen. The system usually comprises two reactors, while one adsorbs the other desorbs nitrogen [55, 46].

The PSA generally works at a pressure between 6 and 10 bar [55]; a pressure of 10 bar is assumed, and a compressor is included in the system to match the hydrogen pressure at 30 bar.

3.6 Sizing

The wind turbine selected for this thesis is a fictitious 300 kW with a 44-rotor diameter. The production target of the plant is 13 tonnes of ammonia a day, similar to other wind to ammonia plants found in literature [46]. The sizing of the components is determined as a result of preliminary simulations and is discussed in the following chapters. The storage size is determined from the final simulation results.

Chapter 4

Numerical Model

Mathematical models are representations of real-world systems used to simplify calculations in complex systems that wouldn't be possible to solve analytically. Once the system components are identified they are translated into mathematical equations that describe the relations between the different variables of the system.

The components of the ammonia plant and their relation are shown in Figure 4.1. The picture also shows how the problem is approached. Two main blocks can be distinguished in the diagram the DOT turbine block and the ammonia production block.

The DOT turbine block, visualized in blue, is composed of the hydraulic turbine, thus wind turbine and high-pressure pump, the RO and the Pelton turbine. This block is responsible for producing a mass flow rate \dot{m}_{H_2O} of desalinated water and power P_{wind} , then divided among the Pelton and the RO.

At every time step t the wind speed U_w is converted into hydraulic power, which is used to generate electricity and desalinated water.

The other block, colored in green, is responsible for the ammonia production. Given that hydrogen production is the most energy-intensive process within the plant, consuming up to 90% of the energy at rated condition according to the scientific literature [46] [44], all generated energy is initially allocated to the PEM. Therefore at the beginning of every time step, during the first iteration:

$$P_{PEM} = P_{wind} \quad (4.1)$$

This allocation of energy will dictate the exact amount of produced hydrogen. Subsequently, following the stoichiometric ratio outlined in reaction 3:1, as shown in Equation 2.2, and the water-hydrogen yield in Equation 4.7, the corresponding amounts of nitrogen and water respectively. These inputs will determine the quantity of ammonia produced and energy expended throughout the cycle.

Finally, once the streams are all determined, the energy consumed by all the components is calculated and the energy to the electrolyzer is recomputed as:

$$P'_{PEM} = P_{wind} - P_{PSA} - P_{comp} - P_{comp}^{rec} - P_{cond} - P_{pump} - P_{RO} \quad (4.2)$$

Where P'_{PEM} is power to the electrolyzer recomputed at the end of the iteration, P_{wind} corresponds to the energy harvested from the wind and $P_{PSA}, P_{comp}, P_{comp}^{rec}, P_{cond}, P_{pump}, P_{RO}$ correspond to the energy consumed by the PSA, compressor, recycle compressor, condenser, pumping work for water (cooling and water pressurization), and RO respectively. The power demand P'_{PEM} calculated at the end of the iteration is compared to initially assigned P_{PEM} . If the energy requirement P_{PEM} closely matches available energy P'_{PEM} within a specified tolerance limit:

$$|P'_{PEM} - P_{PEM}| < TOL \quad (4.3)$$

where TOL is the tolerance and it is equal to 5 kW, the simulation proceeds to the next time step, taking in a new wind input. If the condition of Equation 4.3 is not satisfied P_{PEM} is scaled down. Consequently,

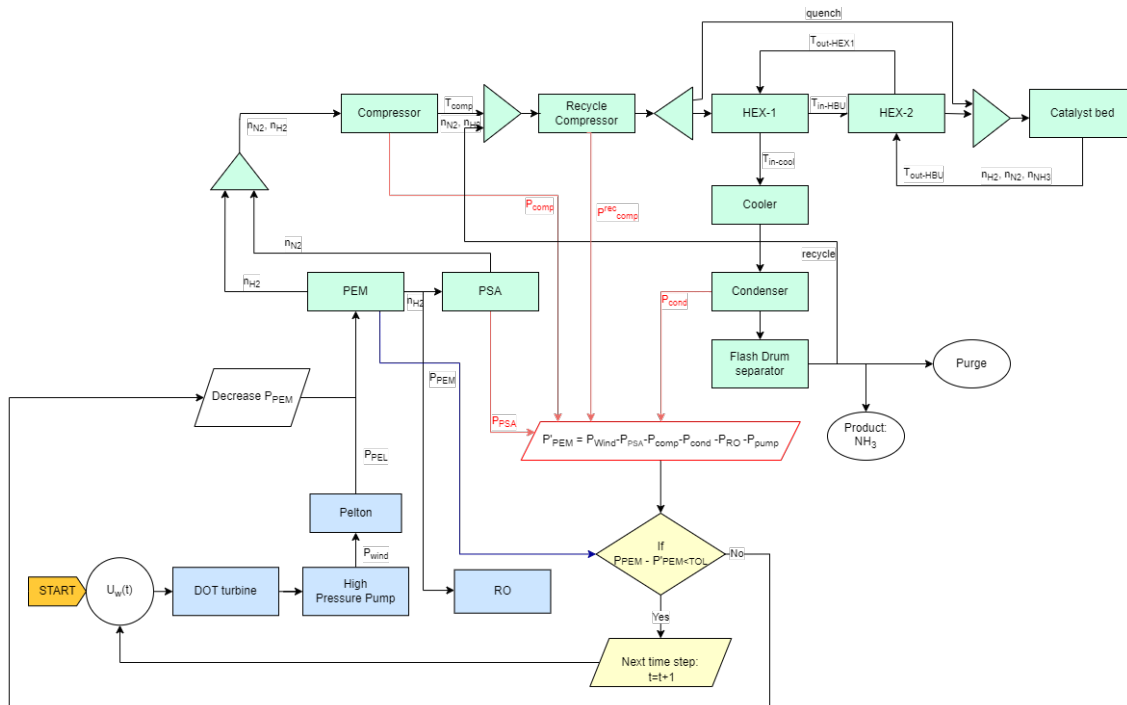


Figure 4.1: Approach

this adjustment cascades to lower the total energy requirements of the entire plant. If after five iterations the condition is not satisfied the simulation does not converge. The results are assumed equal to the previous time step and the simulation skips to the next time step.

Regarding the operation of a **HB** at variable load, the ramp-up of the process is limited by 20% of the nominal load per hour [33]. This limit is implemented in the structure described. The load of the plant refers to the maximum load in the plant during each time step, and correspond to the sum between recycle stream and feed:

$$m_{load} = m_{recycle} + m_{H_2} + m_{N_2} \quad (4.4)$$

Where m_{load} is the load in kg, $m_{recycle}$ is the recycle in kg, m_{H_2} is the hydrogen mass produced in kg, m_{N_2} is the mass of nitrogen produced in kg, all the variable are referred to the time step considered. At each time step the simulation returns the produced amount of ammonia given the wind conditions.

4.1 DOT turbine block

This block consists of 3 modules, the wind turbine, the Pelton turbine and the **RO**. For the wind turbine, a simple wind production curve is used. For simplicity, all the power gathered by the turbine is assumed to be transformed into hydraulic power.

4.1.1 Wind turbine

The modeling of the wind turbine is as simplification. The actual **DOT** power curve would mean including the programming of the control strategy because the hydraulic power in terms of flow and pressure is determined by nozzle opening, water splitting between systems and pump **rpm**. Modelling the control and therefore the wind to hydraulic energy is beyond the scope of the thesis.

The energy of the wind is transformed into hydraulic energy according to the production curve of the turbine as shown in Figure 4.2.

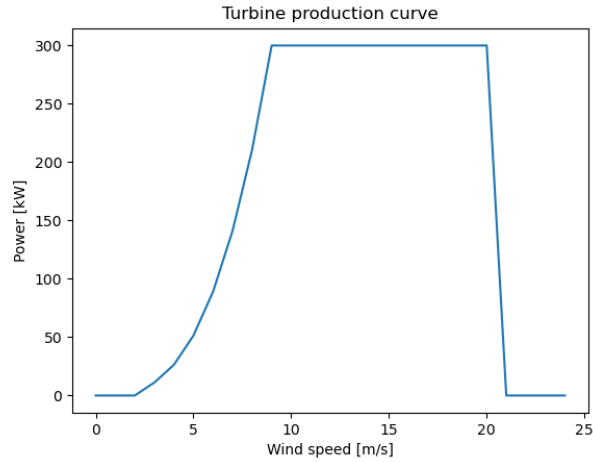


Figure 4.2: Wind production curve

Between cut-in and rated speed the energy is calculated according to Equation 4.5, where ρ is the density of the air, c_p is the power coefficient, an adimensional parameter here considered constant and equal to 0.4421, R is the radius of the turbine and U the wind speed in m/s .

$$P_{wind} = \frac{1}{2}\pi\rho c_p R^2 U^3 \quad (4.5)$$

Between rated and cut-out speed the production is constant and equal to $350kW$. The value of cut-in, rated and cut-out speed are respectively 3, 9 and 20 m/s .

4.1.2 RO

RO is a membrane based desalination technique. Osmosis is a natural process in which water molecules move through a semipermeable membrane from a solution with a low solute concentration (low osmotic pressure) to a solution with a high solute concentration (high osmotic pressure), as shown on the left in Figure 4.3. Due to the membrane's semi-permeability, only water molecules may travel through it,

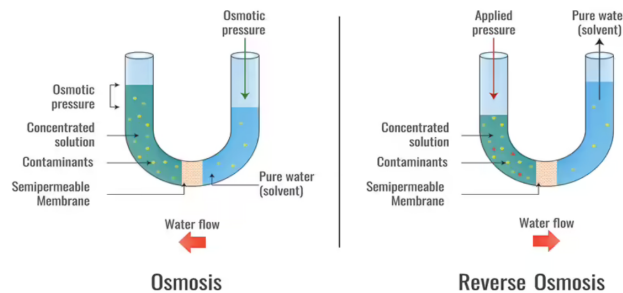


Figure 4.3: On the left osmosis. On the right reverse osmosis [5].

rejecting all other solutes. When the chemical potentials across the membrane are equal, the osmosis process is said to have reached an equilibrium condition. The flow of water molecules can be reversed by applying external pressure on the solution of higher concentration. If the applied pressure difference

is larger than the difference in osmotic pressure across the membrane, molecules flow in the opposite direction from that of the natural osmosis process [16].

The hydraulic power necessary to obtain a certain flow of water \dot{m}_w is proportional to the pressure difference, which drives the water through the membranes.

$$P_{ro} = \frac{\dot{m}_w \Delta p 10^{-5} 10^{-3}}{3600} \quad (4.6)$$

With P_{ro} the hydraulic power necessary for the reverse osmosis in kW , \dot{m}_w the flow of desalinated water in kg/h , Δp the pressure difference in bar.

For the pressure difference a constant value of 70 bar is assumed. The value corresponds to the rated pressure of the membranes [16].

4.1.3 Proton Exchange Membrane

Hydrogen is produced in the electrolyzer through water splitting $2H_2O \rightarrow 2H_2 + O_2$

Two molecules of water are required to produce 2 molecules of hydrogen, the molar ratio is 1:1. Considering the molecular weight of water and hydrogen, respectively 18 and 2 $kg/kmol$, this leads to the following yield where 9 kg of water are necessary to obtain 1 kg of hydrogen:

$$\dot{m}_{H_2} = 9\dot{m}_{H_2O} \quad (4.7)$$

Where \dot{m}_{H_2} , \dot{m}_{H_2O} are the mass flow rate of hydrogen and desalinated water.

Being water electrolysis and endothermic process, energy is required to break oxygen-hydrogen bonds. The PEM is modelled by using a reference value of power consumption $cons_{PEM}$ [6] [56] resulting in the following yield equation:

$$\dot{m}_{H_2} = \frac{P_{PEM}}{cons_{PEM}} \quad (4.8)$$

Where \dot{m}_{H_2} is the mass flow rate in $\frac{kg}{h}$, P_{PEM} is the electrical power applied to the electrolysis cell in kW and $cons_{PEM}$ is equal to $46.73 \frac{kWh}{kg_{H_2}}$.

4.1.4 Pressure Swing Adsorber

Air is composed for 78% of nitrogen [57], thus the amount of nitrogen produced in the ASU

$$\dot{n}_{air} = 0.78\dot{n}_{N_2} \quad (4.9)$$

4.1.5 Nitrogen production consumption

Similarly to PEM, PSA is modelled through reference power consumption value [6] [56], the mass flow rate is then given:

$$\dot{m}_{N_2} = \frac{P_{PSA}}{cons_{PSA}} \quad (4.10)$$

Where \dot{m}_{N_2} is the mass flow rate in $\frac{kg}{h}$, P_{PSA} is the electrical power applied in kW and $cons_{PSA}$ is equal to $0.2 \frac{kWh}{kg_{H_2}}$.

4.2 Ammonia production block

The core of the code lies within the ammonia synthesis block. The subsequent section of the code models the catalyst bed, heat exchanger, condenser, and compressor.

4.2.1 Compression

Before entering the Haber Bosch reactor both nitrogen and hydrogen need to be compressed.

To calculate the amount of power needed, an isentropic compression is considered together with an isentropic efficiency:

$$W_{comp} = \frac{W_{comp, is}}{\eta_{is}} \quad (4.11)$$

Where W_{comp} is the compression work in, $W_{comp, is}$ is the isentropic compression work and η_{is} is the isentropic efficiency.

The work of compression is given by:

$$W_{is} = H_{out, is} - H_{in} \quad (4.12)$$

$$= mc_{p, gas}(T_{out, is} - T_{in}) \quad (4.13)$$

$$= mc_{p, gas}T_{in}\left(\frac{T_{out, is}}{T_{in}} - 1\right) \quad (4.14)$$

Where H denote the enthalpy of the system in $\frac{kJ}{kg}$, m is the compressed mass in kg , $c_{p, gas}$ is the specific heat of the gas mixture in $\frac{kJ}{kg K}$, defined as:

$$c_{p, gas} = \sum_i c_{p, i}x_i \quad (4.15)$$

Where i are the component of the mixture and x the weight fraction, T_{in} and $T_{out, is}$ and respectively the inlet and outlet temperature of the mixture entering and exiting the compressor.

To be isentropic the transformation is assumed adiabatic and reversible. As the gases are assumed to be ideal, the temperature ratio between inlet and outlet can be written as function of the compression ratio:

$$\frac{T_{out, is}}{T_{in}} = \left(\frac{P_{out}}{P_{in}}\right)^{\frac{R}{c_{p, gas}}} \quad (4.16)$$

Where $T_{out, is}$ is the outlet temperature in K of the gases in the isentropic compression. T_{in} is the inlet temperature in K of the gases in the compressor. P_{out} is the outlet pressure in bar. P_{in} is the inlet pressure in bar. R is the gas constant. $c_{p, gas}$ is the specific heat of the mixture as calculated in Equation 4.15. Substituting Equation 4.16 in Equation 4.14 :

$$W_{is} = mc_{p, gas}T_{in}\left[\left(\frac{P_{out}}{P_{in}}\right)^{\frac{R}{c_{p, gas}}} - 1\right] \quad (4.17)$$

Considering the isentropic efficiency the real work can be calculated:

$$W_{comp} = \frac{mc_{p, gas}T_{in}\left[\left(\frac{P_{out}}{P_{in}}\right)^{\frac{R}{c_{p, gas}}} - 1\right]}{\eta_{is}} \quad (4.18)$$

Deriving the equation in respect of time the power consumption is given. Considering the pressure ratio constant, thus the terms in Equation 4.16, the only term that is derived is the mass:

$$P_{comp} = \frac{d}{dt}\left(\frac{1}{\eta_{is}}mc_{p, gas}T_{in}\left[\left(\frac{P_{out}}{P_{in}}\right)^{\frac{R}{c_{p, gas}}} - 1\right]\right) \quad (4.19)$$

$$= \frac{dm}{dt}\frac{1}{\eta_{is}}c_{p, gas}T_{in}\left[\left(\frac{P_{out}}{P_{in}}\right)^{\frac{R}{c_{p, gas}}} - 1\right] \quad (4.20)$$

$$= \dot{m}\frac{1}{\eta_{is}}c_{p, gas}T_{in}\left[\left(\frac{P_{out}}{P_{in}}\right)^{\frac{R}{c_{p, gas}}} - 1\right] \quad (4.21)$$

Where P_{comp} is the compression power in kW , \dot{m} is the mass flow rate of the gas mixture in $\frac{kg}{s}$:

$$\dot{m} = \dot{m}_{H_2} + \dot{m}_{N_2} \quad (4.22)$$

The effective temperature at the outlet of the compressor is given by:

$$T_{out} = T_{in} + \frac{P_{comp}}{\dot{m}c_{p,gas}} \quad (4.23)$$

The isentropic efficiency η_{is} is equal to 0.7.

4.2.2 Heat exchanger

As the reactor is autothermic no external heat input is needed, except for turning on the reactor which is out of the scope of this project. The reactant stream is heated up by the reacted one exiting the catalyst bed, thus exploiting the heat generated in the exothermic reaction.

The streams enter two counter current heat exchanger.

Both heat exchangers are modeled using the $\epsilon - NTU$ method [45]:

$$T_{s_{out}} = \epsilon T_{in} + (1 - \epsilon)T_{s_{in}} \quad (4.24)$$

Where $T_{t_{in}}$ is the catalyst bed outlet temperature (warm gases), while with T_s denominates the cold reactant. ϵ is the heat exchange effectiveness, a parameter that depends on the configuration of the heat exchanger and on characteristic of the warm and cold stream, and that quantifies the percentage of heat, over the maximum available heat, that is transferred. It usually ranges between 0.4 and 0.8 [45], its value has been fixed to 0.65, meaning that 65% of the maximum available heat is transferred.

4.2.3 Catalyst bed

After the mixture has been heated up, ideally in a range of temperature between 500 – 600K, it is ready to enter the catalyst beds.

The steady state material and energy balance for the iron oxide catalyst particles in catalyst beds are shown in Equation 4.25 and 4.26, respectively [46] [45]:

$$\frac{dF_i}{dV_{cat}} = \nu_i r'_{NH_3} \quad (4.25)$$

$$\sum F_i C_{p,i}(T) \frac{dT}{dV_{cat}} = -r'_{NH_3} \Delta H_R(T) \quad (4.26)$$

where F_i is the molar flow rate of species i in $mol s^{-1}$, V_{cat} is the catalyst volume in m^3 , r'_{NH_3} is the rate of reaction $kmol m^{-3} s^{-1}$, ν_i is the stoichiometric coefficient, T is the temperature in K, C_p , is the specific heat capacity of species i in $kJ kmol^{-1} K^{-1}$ and ΔH_R is the heat of reaction in $kJ kmol^{-1}$.

$$r'_{NH_3} = k_T \left(K_f^2 f_{N_2} \left(\frac{f_{H_2}^3}{f_{NH_3}^2} \right)^\alpha - \left(\frac{f_{NH_3}^2}{f_{H_2}^3} \right)^{1-\alpha} \right) \quad (4.27)$$

$$k_T = k_0 \exp\left(-\frac{E_a}{RT}\right) \quad (4.28)$$

$$f_i = y_i \phi_i p \quad (4.29)$$

The reaction kinetics are modelled using the Temkin equation [46] [45] described by Equations 4.27 4.28; where k_T is the rate constant in $atm^{0.5} h^{-1}$; K_f is the equilibrium constant in atm^{-1} ; α is a dimensionless

parameter specific to the catalyst; k_0 is the pre-exponential factor in $atm^{0.5}h^{-1}$; E_a is the activation energy in $kJkmol^{-1}$; R is the ideal gas constant. The fugacity, f_i , of each component is calculated using Equation 4.29, where y_i and ϕ_i are the mole fraction and fugacity coefficient of i -component respectively and p is the pressure in atm . Due to the selected catalyst size (2–3 mm), the rate of reaction can be taken without a corrective factor and the pressure drop can be neglected [46].

In the following Table 4.1 the constants of the industrial catalyst ZA-5, used to evaluate the rate of reaction, are reported.

	ΔT_{cool}
α	0.5
$E_a [\frac{kJ}{kmol}]$	1.5910^5
$k_0 [\frac{atm^{0.5}}{s}]$	$4.97310^{12}10^0.53600$

Table 4.1: ZA-5 wustite catalyst parameters

The dimension of the first and second bed is set to $0.3m^3$ and $0.6m^3$, according to [44], due to its similar nominal output.

Relation from ΔH and $\dot{n}_{quench,1} = u_1 \dot{n}_{in}$, $\dot{n}_{quench,2} = u_2 \dot{n}_{in}$, $\dot{n}_{quench,3} = u_3 \dot{n}_{in}$

The quench fractions u_1, u_2, u_3 are adjusted via Trial-and-error for the highest efficiency of the plant and are respectively 0.4, 0.2 and 0.4.

Then, the quench stream 2 and 3 will be mixed with the stream entering the first and second catalyst bed respectively. Their temperature and mole fraction is described with the Equations 4.35 and 4.36 [32]:

$$T_{out} = \frac{\dot{n}_{in1}}{\dot{n}_{in1} + \dot{n}_{in2}} T_{in1} + \frac{\dot{n}_{in2}}{\dot{n}_{in1} + \dot{n}_{in2}} T_{in2} \quad (4.35)$$

$$y_{i,out} = \frac{\dot{n}_{in1}}{\dot{n}_{in1} + \dot{n}_{in2}} y_{i,in1} + \frac{\dot{n}_{in2}}{\dot{n}_{in1} + \dot{n}_{in2}} y_{i,in2} \quad (4.36)$$

Where 1 and 2 denote the 2 mixing streams.

4.3 Power Production and Consumption

When referring to a system as "stand-alone," it implies that the plant is self-sustaining and does not rely on external energy inputs. In this context, all electricity utilized within the components originates exclusively from the Pelton turbine. In order to maximize the energy utilization, the following equations ought to be satisfied at each time step:

$$P_{pel} = P_{PEM} + P_{PSA} + P_{comp} + P_{comp}^{rec} + P_{cond} + P_{pump} \quad (4.37)$$

$$P_{wind} = P_{pel} + P_{RO} \quad (4.38)$$

In Equation 4.37 the electricity balance with the power produced by the Pelton turbine P_{pel} on the left-hand side, and the energy consuming component on the right-hand side, P_{PEM} the electrolyzer, P_{PSA} the ASU, P_{comp} the feed compressors, that comprise the nitrogen compressor and the hydrogen-nitrogen compressor, P_{comp}^{rec} recycle compressor, P_{cond} the condenser, P_{pump} the pump, which supply compressed water to the electrolyzer and ensure water for cooling through the system.

In Equation 4.38 the energy harvested by the wind turbine P_{wind} on the left-hand side, balances with the energy from the Pelton turbine P_{pel} and RO P_{ro} , on the right-hand side.

4.4 Simulation time

For the catalyst bed the differential equations were initially solved by using the Python solver "odeint". Due to the high computational time the solver has been substituted with a simpler and less accurate vector operations, which significantly speeds up computation time, roughly 18 seconds for the solver while the vector operations takes roughly 7 seconds.

$$F_i(V) = F_i(V - 1) + \nu_i r'_{NH_3}(T(V - 1), F(V - 1))dV \quad (4.39)$$

$$T(V) = T(V - 1) - r'_{NH_3}(T(V - 1), F(V - 1)) \frac{\Delta H_R(T(V - 1))}{\sum F_i(V) C_{pi}(T - 1)} dV \quad (4.40)$$

Where $F_i(V)$ is the molar flow rate in kmol/h of the i-element along the catalyst volume, ν , r'_{NH_3} , C_{pi} , ΔH_R are respectively the stoichiometric coefficient, the rate of reaction, specific heat capacity and heat of reaction, calculated as described in Section 4.2.3.

The results obtained with the solver and the vectorial form are compared and shown in the Table 4.2. The table report the temperature T in K, and the molar fraction y at the inlet and outlet of the beds.

1 st catalyst bed	input	reference output	ZA-5	ZA-5 vector
T[K]	673	773	741.45	720.74
y_{N_2}	0.6812	0.6369	0.6511	0.6389
y_{H_2}	0.2271	0.2123	0.2170	0.2130
y_{NH_3}	0.0417	0.0981	0.07989	0.0954
y_{Ar}	0.05	0.0527	0.0518	0.0525
time[s]	-	-	18.49	7.09

2 nd catalyst bed	input	reference output	ZA-5	ZA-5 vector
T[K]	673	772.93	717.05	703.97
y_{N_2}	0.6524	0.6031	0.6324	0.6241
y_{H_2}	0.2174	0.2010	0.2107	0.2079
y_{NH_3}	0.0784	0.1411	0.1037	0.1144
y_{Ar}	0.0518	0.0548	0.0530	0.0535

3 rd catalyst bed	input	reference output	ZA-5	ZA-5 vector
T[K]	673	760.01	697.80	689.93
y_{N_2}	0.6254	0.5779	0.6137	0.6094
y_{H_2}	0.2084	0.1926	0.2045	0.2030
y_{NH_3}	0.1128	0.1732	0.1210	0.1330
y_{Ar}	0.0534	0.0563	0.0541	0.0543

Table 4.2: Simulation time: comparison between differential equation solver and vectorial form.

4.5 Code validation

The results of each function, representing a component of the plant, are validated with literature. Once each block has been individually validated, the overall performance of the plant is assessed.

For the catalyst bed the code has been validated with results obtained by Cheema et al. [45]. Using the same inputs for temperature, mole fraction and bed length, the simulation is repeated twice with

difference catalyst parameters, the simulation is repeated twice with different catalyst parameters. In the first case the same catalyst described in [45] is used, a traditional magnetite catalyst. In the second case, the parameters of the selected catalyst, an iron oxide catalyst, ZA-5 [46], are used. The results obtained in both cases are more conservative, especially for the ZA-5 in the second and third beds, so they are considered acceptable and realistic.

In Table 4.3 the reference results and the result obtained for every bed are shown.

1 st catalyst bed	input	reference output	traditional catalyst-vector	ZA-5 vector
T[K]	673	773	721.49	720.74
y_{N_2}	0.6812	0.6369	0.6393	0.6389
y_{H_2}	0.2271	0.2123	0.2131	0.2130
y_{NH_3}	0.0417	0.0981	0.0949	0.0954
y_{Ar}	0.05	0.0527	0.0525	0.0525

2 nd catalyst bed	input	reference output	traditional catalyst-vector	ZA-5 vector
T[K]	673	772.93	705.47	703.97
y_{N_2}	0.6524	0.6031	0.6235	0.6241
y_{H_2}	0.2174	0.2010	0.2077	0.2079
y_{NH_3}	0.0784	0.1411	0.1151	0.1144
y_{Ar}	0.0518	0.0548	0.0535	0.0535

3 rd catalyst bed	input	reference output	traditional catalyst-vec	ZA-5 vector
T[K]	673	760.01	698.34	689.93
y_{N_2}	0.6254	0.5779	0.6021	0.6094
y_{H_2}	0.2084	0.1926	0.2006	0.2030
y_{NH_3}	0.1128	0.1732	0.1423	0.1330
y_{Ar}	0.0534	0.0563	0.0548	0.0543

Table 4.3: Catalyst bed verification data.

The PEM and PSA blocks were built to be compliant with average power consumption from literature [6] [56], thus the blocks do not need further validation.

Compressor, heat exchanger, cooler and condenser have all been validated using the data from Lin et al. [44].

For the compressor input data is shown in Table 4.4. Isoentropic and mechanical efficiency are respectively $\eta_{is} = 0.70$ e $\eta_m = 0.95$, leading to similar results for both outlet temperature and power consumption as shown in Table 4.4.

The heat-exchanger is validated with $\epsilon = 0.64$, the results are compared in Table 4.5.

For cooler and condenser input data for verification are in Table 4.5, the obtained power are respectively $P_{cool} = 2492.40kW$ and $P_{cond} = 1457.21kW$ similar to the results of Lin et al.

Once the modules are verified and put together the code is run to simulate operation at rated power, with constant energy supply.

The overall power usage pictured in is compared to with the one observed in [46] and [44].

Typical large-scale systems achieve up to 26% single-pass conversion and between 97–99% overall conversion with the recycle stream [46] [48].

Compressor	input	reference output	code output
T[K]	673	531.492	517.58
P[kW]	-	1200	1229.56
\dot{m} [kg/h]	2432	2432	2432
x_{H_2}	0.177632	0.177632	0.177632
x_{N_2}	0.822368	0.822368	0.822368
x_{NH_3}	0.0	0.0	0.0

Table 4.4: Compressor verification data

HEX	input	reference output	code output
T_w [C]	479	340	330.76
T_c [C]	127	350	352.64
\dot{m}_w [kg/h]	9520.4	9520.4	9520.4
\dot{m}_c [kg/h]	5712.25	5712.25	5721.25
$x_{H_2}^w$	0.1435	0.1435	0.1435
$x_{N_2}^w$	0.5776	0.5776	0.5776
$x_{NH_3}^w$	0.2787	0.2787	0.2787
$x_{H_2}^c$	0.1888	0.1888	0.1888
$x_{N_2}^c$	0.7874	0.7874	0.7874
$x_{NH_3}^c$	0.0236	0.0236	0.0236

Table 4.5: Heat-exchange verification data

Condenser	ΔT_{cool}	ΔT_{con}	$y_{NH_3}^v$	m_w[kg/h]	x_{H_2}	x_{N_2}	x_{NH_3}
input	281.292	60	0.92	9520.4	0.1435	0.5776	0.2787

Table 4.6: Cooler and condenser verification input data.

The global efficiency of the plant, defined as the ratio between input reactants and output ammonia, is 94.46%, with a conversion efficiency of the first and second bed, respectively, of 25.99% and 17.67%. The feed stream is 30.92% of the total mass rate circulating in the plant, also consistent with Lin et al. [44] where the feed stream accounts for the 25.54% of the total mass.

The total power consumption was 35.01 GJ/tonNH₃ or 9.86 kWh/kg, comparable to 37.4 GJ per metric ton of ammonia calculated by Cunanan et al. [46] and to the one calculated by Lin et al. [44] of 9.70 kWh/kg NH₃.

Energy breakdown is also comparable to the one calculated by [44] and [46], where most of the energy is taken up by the electrolyzer, 91.5% [44] and 88.07% [46].

Figure 4.6 show the power breakdown among components excluding the electrolyzer. More than half of the power consumption showed in Figure 4.6 is taken by the compressors: Feed-Compressor, Rec-Compressor, Nitrogen-Compressor, Water pump. This means that any reduction in the pressure of the system would be beneficial for power consumption. The water pump feeding the electrolyzer is particularly demanding. The desalinated water is assumed to be compressed from 1, at the outlet of RO, to 30 bar for the inlet of PEM.

4.6 Sizing

The component sizing in this power system considers power requirements and the mass or flow rates. Beginning with the feed compressor, rated at 81.23 kW, it handles a mass flow of 584.24 kg, operating

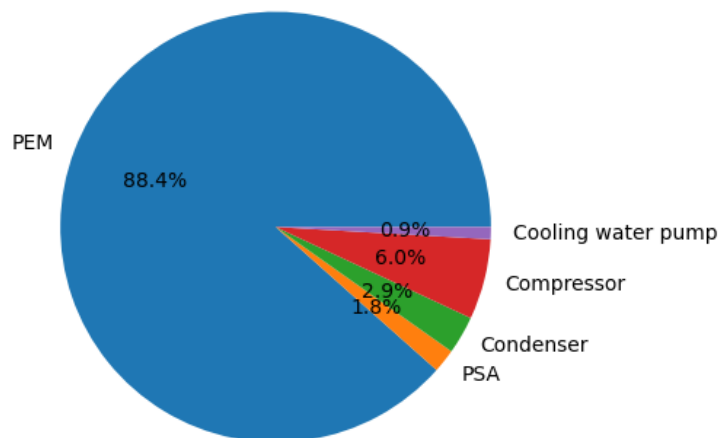


Figure 4.5: Energy break down among plant components

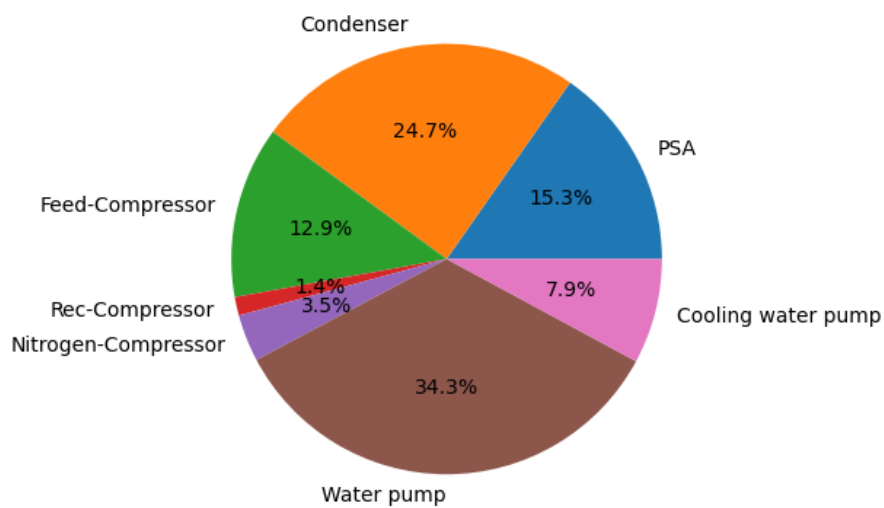


Figure 4.6: Energy breakdown among plants component, excluding the electrolyzer.

within the pressure range of 30 to 82 bar. Subsequently, the recycle compressor, with a power rating of 8.77 kW, accommodates a significantly higher mass flow of 1889.41 kg, tailored for the narrower pressure range of 82 to 85 bar. Similarly, the nitrogen compressor, with a power rating of 22.26 kW, manages a mass flow of 481.20 kg, specifically compressing nitrogen within the range of 10 to 30 bar. Meanwhile, the water compressor, with a substantial power requirement of 216.36 kW, operates at a mass flow rate equivalent to $0.90475 \text{ m}^3/h$, compressing water across the extensive range of 1 to 30 bar. The condenser needs to extract 310.7 kW and manages a mass flow rate of 1889.41 kg/h. For cooling duty a power requirement of 49.67 kW is expected to pump water into the system, and contribute to maintaining optimal temperatures. Lastly the PEM requires 4815 kW, producing at rated 103.041 kg/h of hydrogen. The energy required to produce 13 tons of ammonia in a day is 5340 kWh/day, and 18 of the selected turbines collectively provide 5400 kW. Therefore, the wind farm is composed of 18 turbines.

4.7 Sensitivity Analysis

A sensitivity analysis is performed on the non-linear component and on the overall plant to test the strength of the code.

For the catalyst bed inlet temperature is increased by 10K, hydrogen flow rate is increased by 1%, nitrogen is increased by 1%, ammonia is increased by 1%

1 st catalyst bed	Reference	$T_{in} + 10K$	$y_{H_2} + 0.01\%$	$y_{N_2} + 0.01\%$	$y_{NH_3} + 0.01\%$
T[K]	720.74	715.40	720.90	720.79	720.55
y_{N_2}	0.6389	0.6344	0.6410	0.6372	0.6388
y_{H_2}	0.2130	0.2115	0.2113	0.2148	0.2129
y_{NH_3}	0.0954	0.1011	0.0953	0.9544	0.0956
y_{Ar}	0.0525	0.0528	0.0522	0.0524	0.0525

Similarly, for the compressor, inlet temperature is increased by 10K, hydrogen content is increased of 1%, nitrogen content is increased by 1%. Results are reported in Table 4.7.

Compressor	reference	$T_{in} + 10K$	$x_{H_2} + 0.01\%$	$x_{N_2} + 0.01\%$
T[K]	517.58	543.67	517.66	517.66
P[kW]	1229.56	1270.85	1226.58	1226.58

Table 4.7: Compressor sensibility analysis

For the plant the following inputs are changed: power is decreased by 10%, hydrogen and nitrogen temperature is increased by 10K. Results are shown in Table 4.8.

Plant	reference	P+10%	$T_{in} + 10K$
NH_3^{prod} [kg]	558.92	561.90	554.32
η_{plant}	0.9455	0.9411	0.9377
$conversion_1$	0.2586	0.2587	0.2559
$conversion_2$	0.1755	0.1756	0.1732

Table 4.8: Plant sensibility analysis

Chapter 5

Simulation results of a Wind to ammonia plant without storage

In this chapter, the wind-powered ammonia plant is simulated without storage. The case study is simulated with the wind conditions of Agios Efstratios island, discussed in Section 5.1. The results are presented in Section 5.2.

The simulation is based on the plant illustrated in Figure 3.3.

5.1 Wind Data

The data set used for the simulation is a subset of a data set representative of wind speed on Agios Efstratios, an island located in the Northern Aegean Region. This data set is used for ease of data retrieval, as it has already been used in the DOT thesis "Numerical simulation and operating strategy of a wind-powered electricity and freshwater production system" by Angeliki-Chrysoula Pytharouli [16]. The dataset reflects a year's worth of wind data on the island. It's derived from the examination of wind speeds and their comparison with the wind's characteristics over ten years. Selecting a representative year involves analyzing both weekly and monthly wind values to capture crucial peaks that might be overlooked if wind speeds were solely averaged monthly. To determine the representative year, monthly averages for each year are computed and then averaged across the ten-year period. This process ensures that the resulting representative year aligns with the overall average trend. Additionally, the maximum and minimum weekly values observed throughout the dataset are incorporated to ensure their representation in the chosen year's wind profile.

Due to time constraints the simulation is run over 1 week equivalent to 168 time steps. The data is shown in Figure 5.1. The data consists of hourly wind speeds, which indicates that the system will calculate the ammonia, water, and power production hourly.

5.2 Results

Over the 168 time steps, the simulation converged for every time step and the ramp-up limit was hit once. Figure 5.2 shows power production, divided between the Pelton turbine and the RO module. Despite the disparity in magnitude, the patterns of both the Pelton turbine's power output and the RO process power consumption are visually almost indiscernible. This can be attributed to the proportional relationship between desalinated water production and hydrogen production.

The desalinated water produced by the RO process serves as a crucial input for the electrolyzer, which generates hydrogen through electrolysis. Consequently, as no storage is included, the power consumption

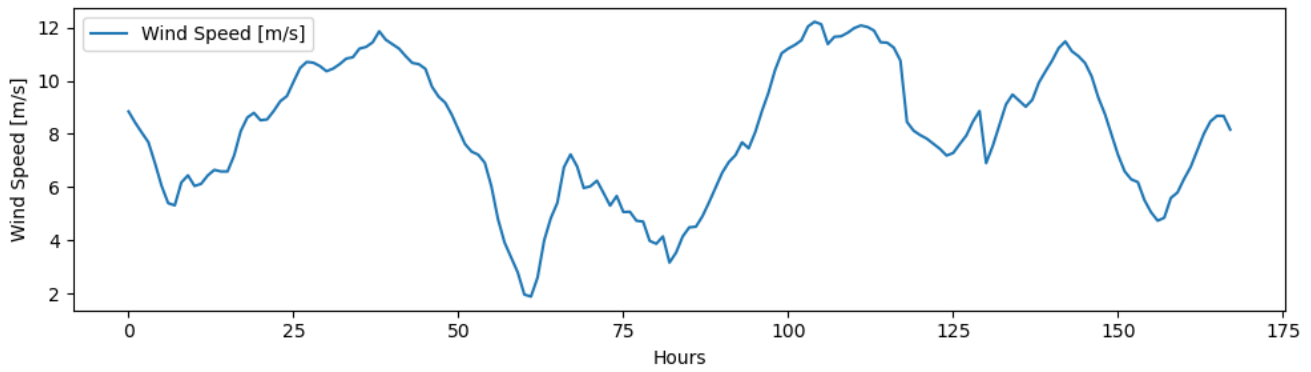


Figure 5.1: Wind speed

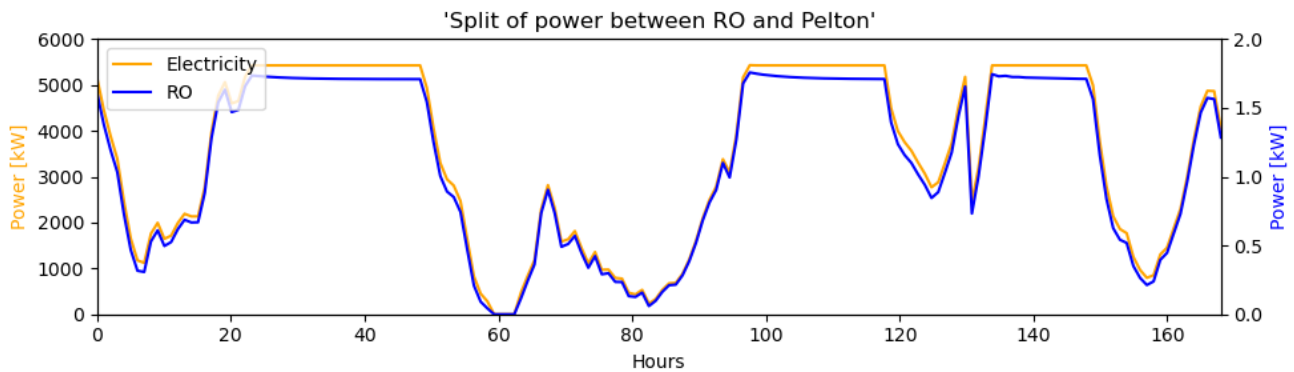


Figure 5.2: Power division among the Pelton and RO per time step.

of the RO, which is directly tied to water production, exhibits a similar trend.

It can be observed that the power required for the RO is relatively small. This means that it is not necessary that all turbines are devoted to water production. Considering eventual backup, three out of twenty turbines in the wind farm would be sufficient and could potentially be dedicated to only water production. For instance, one would already be enough as the PRO system can desalinate water up to $25 \text{ m}^3/\text{h}$ at rated condition [58] and the consumption of water never overcomes the $1 \text{ m}^3/\text{h}$ as shown in Figure 5.3. This also suggests the opportunity that water could be produced in surplus and mostly at rated power, or high wind speed, to be stored and used at lower speed. Moreover, it could allow for an easier control strategy where hydraulic power has to be split only at high wind speed and can be fully devoted to the Pelton turbine for the rest.

Figure 5.4 shows ammonia production in green and the mass flow in the plant at every time step. The ammonia production ranges from 535.54 kg/h when the plant is operating at rated power, so producing 5.4 MWh , to 0 when the wind speed is below cut-in speed. It reveals a similar trend to the Pelton turbine's power output and the RO power consumption, so it follows the wind power output, albeit with smoother variations. This smoothness can be attributed to the presence of a recycle stream, which accounts for 70% of the total load in the plant, see Section 4.5.

The recycle stream in the system plays a significant role in stabilizing ammonia production over time by reintroducing unused reactants and products back into the process. This recycling mechanism helps maintain a more consistent level of reactants within the system, thereby smoothing out fluctuations in production.

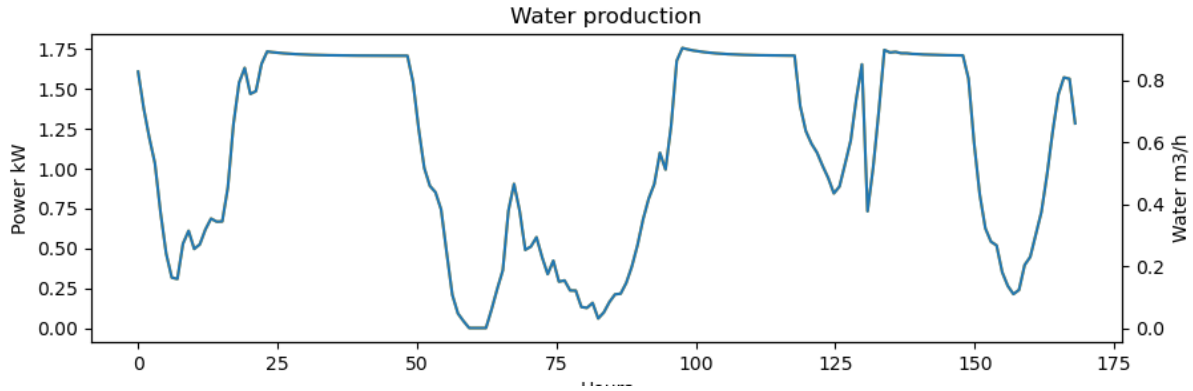


Figure 5.3: Consumption of hydraulic energy and production of water from the RO module.

The total flow, calculated as in Equation 4.4, in the plant is also shown in the purple line of Figure 5.4. The orange and red lines highlight when the flow goes below 50% of the load and 20% respectively. Industrial ammonia plants don't go below 50% of the nominal load [33], this would also benefit other components, such as the compressor, which also operates down to 50% of flexibility. However, with a control strategy on the inlet temperature of the bed it is possible to go down to 10% - 20% according to [33].

The minimum load is relevant not only in regard to the flexibility of the components but also for heat losses. These are not taken into account in the model, as in all the HB model found in literature, but could play a significant role as the load decreases[45], causing the temperature to drop too far so to slow down the reaction and to shut down the system.

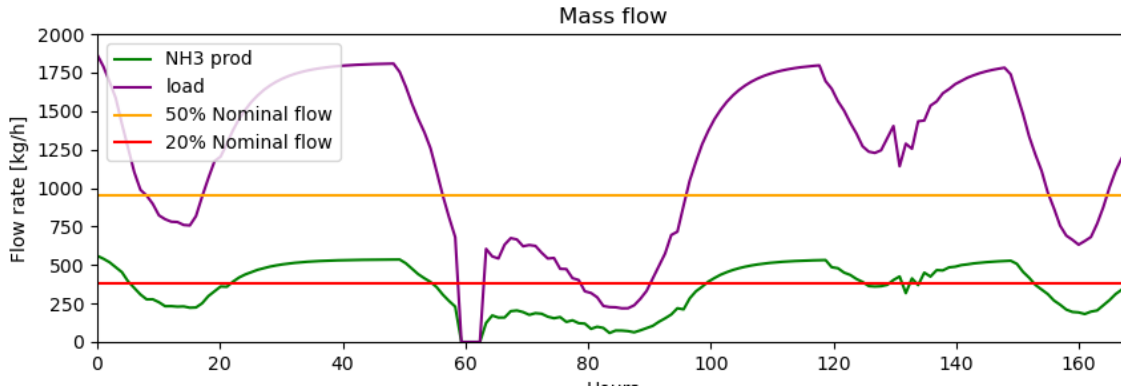


Figure 5.4: Mass flow rate of produced ammonia and total mass flow of the plant per time step.

In Figure 5.5 the ratio between the energy content of the ammonia produced and the wind energy harvested by the turbine is shown:

$$\eta = \frac{m_{NH_3} e_{NH_3}}{E_{wind}} \quad (5.1)$$

Where m_{NH_3} is the mass of ammonia produced in the time step in kg, e is the energy density of ammonia in kJ/kg, and E_{wind} is the Energy harvested by the wind turbine in kJ.

The η is equal to 0.6778 at the rated condition, meaning that 67.78% of the energy harvested by the wind turbine is stored into ammonia and have the meaning of an efficiency. The value initially increases when P_{wind} decreases. This is due to the beneficial effect of the recycle stream. A reduction in available

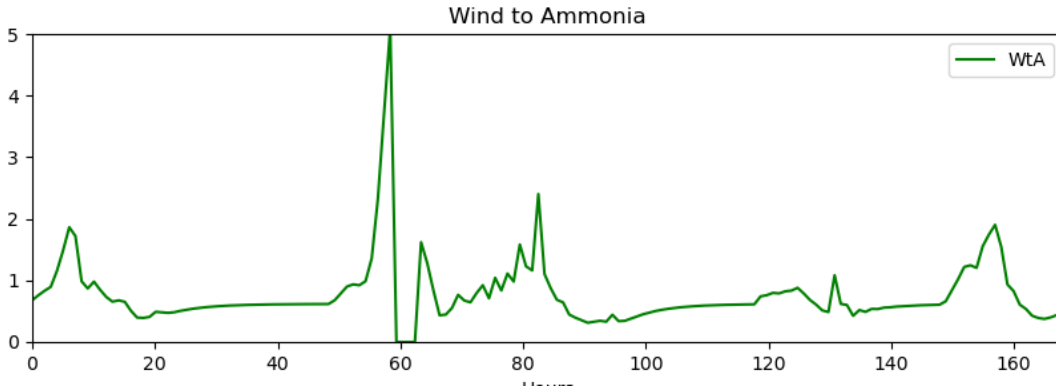


Figure 5.5: Wind to Ammonia. Energy obtained from produced ammonia over harvested wind energy per time step.

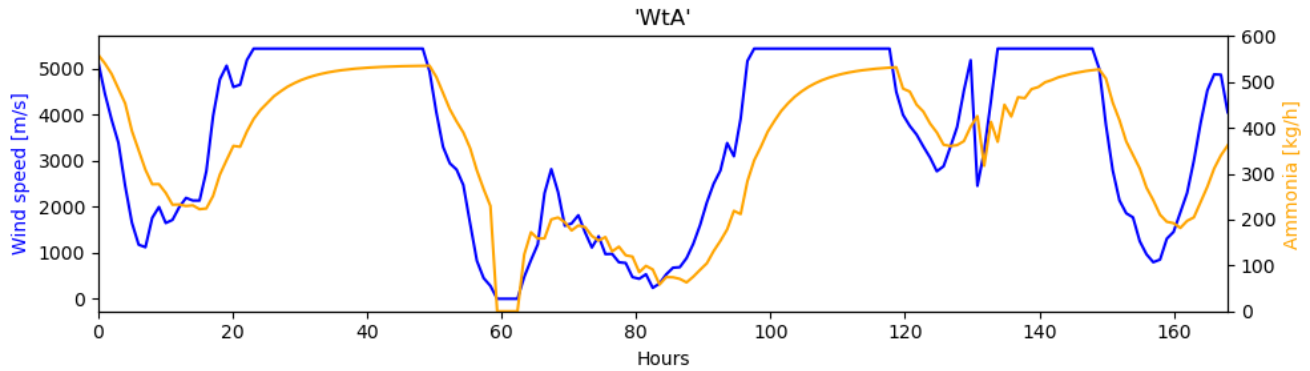


Figure 5.6: Wind power and ammonia production per time step.

P_{wind} causes a reduction of the feed gases, which, at rated conditions accounts only for 30% of the total gases circulating in the plant 4.5. First, the recycle stream is high enough to increase the efficiency, but then the efficiency drops quickly when the recycle stream stabilize to lower loads. Between time steps 60 and 64 the value is 0 as $P_{wind} = 0$ and no ammonia is produced.

The relationship between the power harvested by the turbine and ammonia production in the HB is shown in Figure ???. The production follows the general trend of wind speed. As wind speed increases, there is a tendency for ammonia production to also increase. The plateau in ammonia production corresponds to a plateau in the wind turbine production curve. This plateau occurs because as wind speed increases, there's a point where the wind turbine reaches its maximum capacity and cannot generate additional power, thereby limiting the amount of energy available for the ammonia production process. It is also noteworthy that while wind speed fluctuates, the trend in ammonia production appears smoother. The responsible factor for this behavior is attributed to the presence of the recycle stream. This buffering effect helps mitigate the direct impact of fluctuations in wind speed on the ammonia production rate, resulting in a smoother overall production trend.

The capacity factor of the plant is calculated as in Equation 5.2 and is 0.6323.

$$C_F = \frac{\sum m_{NH_3}(t)}{m_{rated}T_{tot}}$$

Where \dot{m} is the mass of produced ammonia at each time step in kg, m_{rated} is the mass of ammonia produced at rated condition in one hour, T_{tot} is the total number of hour through the plant is simulated.

As a final consideration, it is noted that the observed load fluctuations in the simulation are potentially

unrealistic, as real-world components have inherent limitations in flexibility. Especially the cooling down of the bed, when the plant is not able to operate due to wind speed being lower or very close to cut-in speed, can cause the reactor to shut down. The necessity for storage operate when will be further evaluated in the subsequent chapter.

Chapter 6

Simulation results of a Wind to ammonia plant with storage

In this chapter, the wind to ammonia plant is simulated and analyzed on the same wind data presented in Chapter 5, albeit with a focus on incorporating storage systems. Specifically, simulations are presented that integrate storage solutions in form of batteries for electricity and water tanks for desalinated water. The simulation is later extended to include the integration of a hydrogen tank. In Figure 6.1 the schematic of the plant with storage is shown.

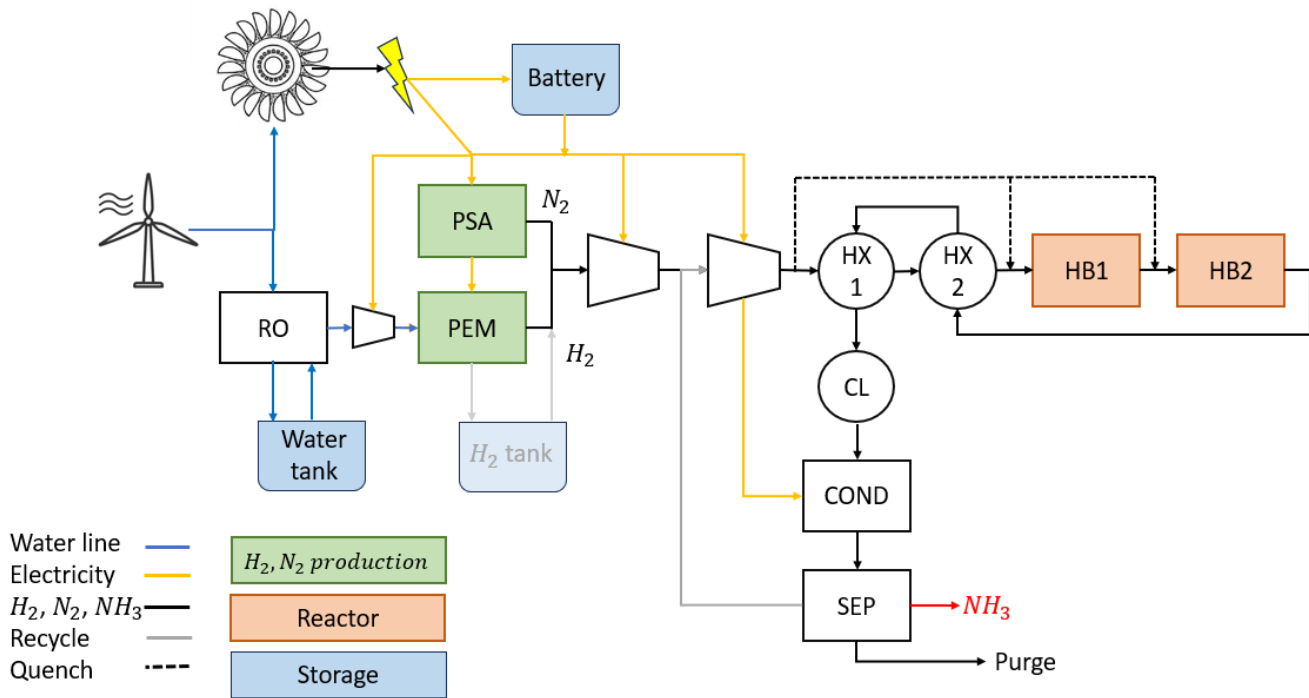


Figure 6.1: Plant schematic with battery, water tank and hydrogen tank included.

The storage system is included and sized to facilitate the sustained operation of the HB process. While other components are modelled as ideal, as flexible and capable of a continuous dynamic response, the current emphasis is solely on optimizing the continuity of the HB process. It is assumed that heat losses are negligible down to $m_{load} = 20\%m_{rated}$.

6.1 Electrical Storage

A battery of 1000 kWh is included in the model. The battery control is simple to facilitate results interpretation. The battery charges when P_{wind} surpasses a precise threshold, called P_{char} , and discharges when the mass load going through the plant goes below a certain percentage of the nominal load. The load refers to the highest flow rate going through the plant, the sum of the produced gases, and the recycle stream.

The minimum load of the plant is scaled down from 50% to 20% of the nominal load, to assess its impact on the plant's ability to sustain continuous operation. By altering the minimum load threshold, we aim to investigate how changes in operational parameters affect the utilization of storage systems and the overall performance of the plant.

By introducing the storage solutions, Equation 4.37 needs to be modified as follows:

$$P'_{PEM} = (P_{wind} - P_{PSA} - P_{comp} - P_{comp}^{rec} - P_{cond} - P_{pump} - P_{RO}) - P_{storage}^{el} \quad (6.1)$$

where $P_{storage}^{el}$ is positive when the storage is charging and negative when is discharging.

6.2 Water Storage

A tank is implemented to store water. The tank is filled when P_{wind} overcomes a certain threshold, and discharges when P_{wind} is below it. The strategy implemented here is to maximize water production at high wind speeds, when more wind power is available, and avoid production at lower speeds, so that all wind power can be used as electricity (directing all the seawater flow to the Pelton turbine) to power the ammonia plant components. The introduction of water storage is not expected to have much influence on the operation of the rest of the plant, given its minimal power consumption, as was shown in Figure 5.3. However, its presence can give important insights for the operation of the DOT turbine and it is deemed necessary for the actual operation of the RO membranes.

The water tank size is initially set to $10m^3$, 1 kW of hydraulic power is devoted for RO at each time step. The storage input are shown in 6.2

$P_{char} [kW]$	5350
$P_{disch}^{RO} [kW]$	4000
$P_{storage}^{RO} [kW]$	1
$P_{storage}^e [kW]$	$P_{wind} - P_{char}$

Table 6.1: Storage input

6.3 Results without hydrogen storage

The Pelton turbine and the Reverse Osmosis (RO) system are no longer directly interconnected. The RO now operates intermittently, consuming power ranging between 1.5 and 3 kW. Although the power production of the RO remains relatively low, there is potential for further optimization and enhancement.

From the first set of storage simulation it is determined that a water tank of $15m^3$ with a $P_{charge} = 5350kW$ and a $P_{discharge} = 4000kW$ is sufficient to provide desalinated water during the low-speed period as can be seen in Figure 6.2. The RO operates independently of the Pelton turbine's power output, shifting the production in the high wind speed region. The tank discharges four times over one week, with the lowest SOC equal to 29.60%.

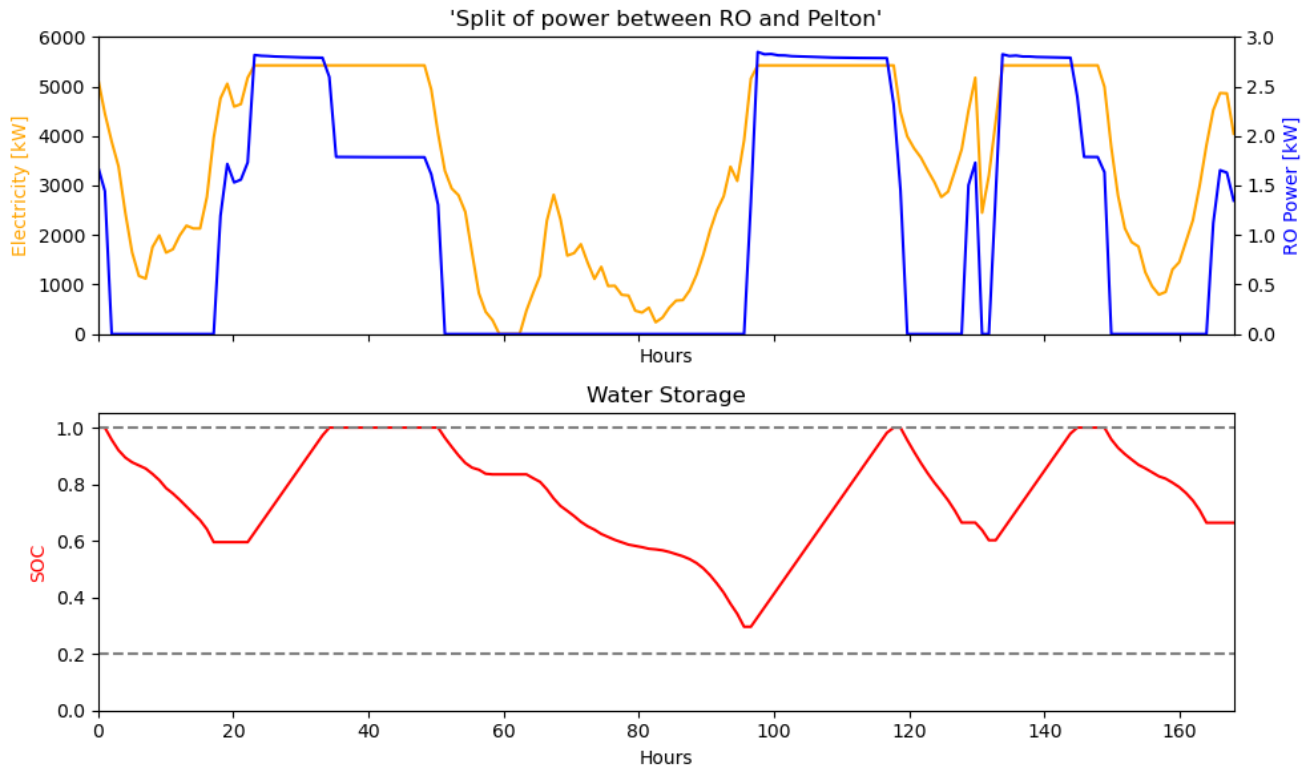


Figure 6.2: On top power distribution between Pelton and RO. On the bottom, the water tank charging/discharging, size $15m^3$.

Discharging, set at $P_{wind} < 4000kW$ is met when wind speed drops below 8.14 m/s.

In Figure A.3 the battery and the load of the plant are pictured. The battery is able to fully recharge when $P_{charge} = 5350kW$. The battery quickly discharges when the load goes below the threshold, shown in red, and it is not able to maintain the plant operation over the minimum load.

Even when the minimum load is set at 20%, Figure 6.3, the battery is not able to withstand periods with no power production.

6.3.1 Storage Control Strategy

Results show that charging the electrical storage only when energy production is high is not enough to withstand long low-speed periods. For this reason, a different control strategy is implemented aiming to recharge the storage as soon as possible. The strategy operates the plant at the minimum load when $SOC_e < 1$, and uses the power surplus to recharge the battery.

The following Figures 6.4, A.7, A.6, A.5 highlight that the battery starts supplying energy as soon as the minimum load is hit. Nevertheless, the battery is not enough to sustain the operation of the plant even at lower loads as 20% in Figure 6.4.

The production of ammonia between time steps 60 and 80 appears to be nearly identical to the scenario without storage.

Smaller battery sizes, 100kWh and 500kWh have been tested with negative results. The battery has not been further increased as 1000kWh is already 18.5% of the installed capacity.

This result is not unexpected as batteries are well known short term storage system. Batteries have

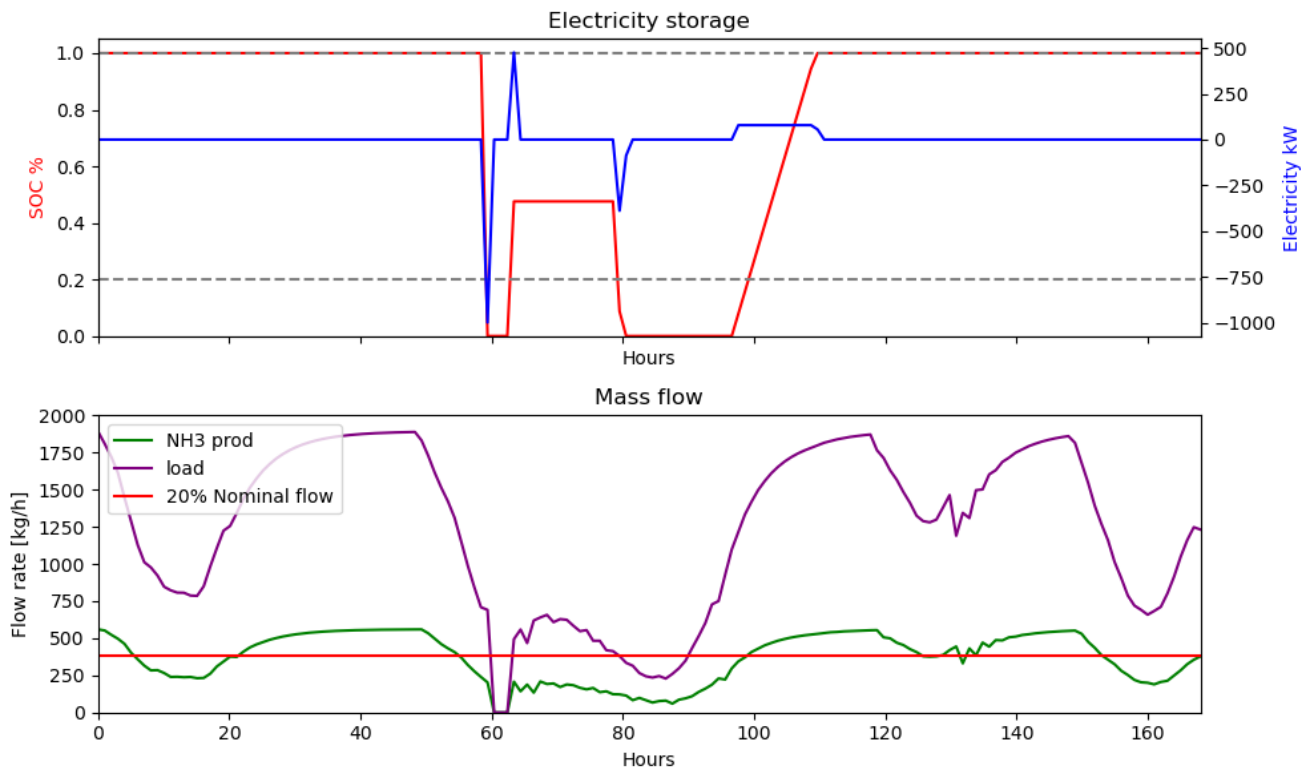


Figure 6.3: On top 1000kW battery charging/discharging. On the bottom the mass flow in the plant and the ammonia produced. The battery discharges when the load goes below 20% and charge when $P_{wind} > P_{char}$.

a good response over seconds or minute of operation and their response may not be clearly visible due to the hourly time scale of the wind data. Batteries are short time storage, effective to improve the stability of the load. However, to successfully sustain production for longer time, it would need to be oversized. Therefore its inability to run the electrolyzer on its own. Hydrogen needs to take the place for long term (large) capacity storage.

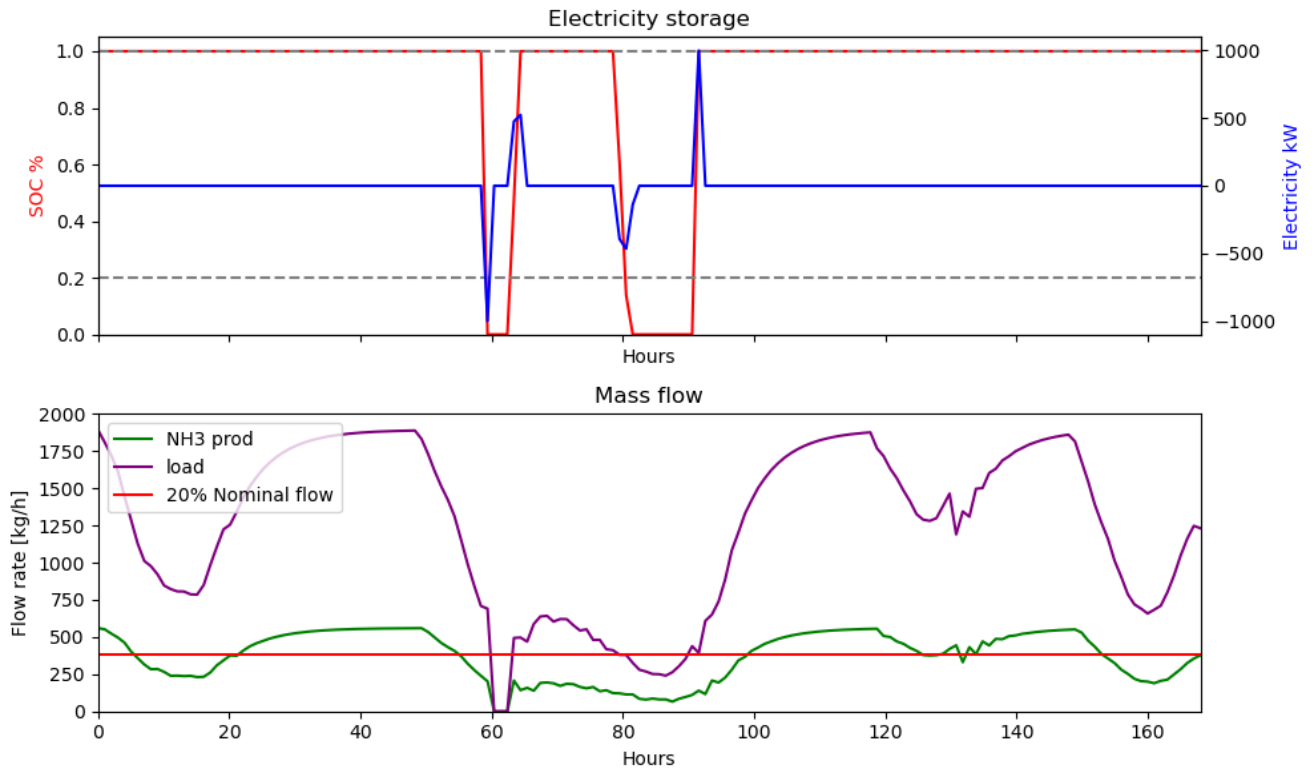


Figure 6.4: On top battery charging/discharging. On the bottom the mass flow in the plant and the ammonia produced. The battery discharges when the load goes below 20% and charge when $SOC < 1$

6.4 Hydrogen Storage

As electricity storage is not able to provide enough power to sustain constant production, hydrogen storage is implemented. Hydrogen production is the most energivorous process in the plant, taking up almost 90% of the total energy consumption. If the tank can supply the required hydrogen to sustain the cycle during periods of low-wind speeds, the battery's role shifts to providing energy solely for the operation of other components. These additional components typically account for approximately 10% of the total energy consumption, see Section 4.5.

The hydrogen tank will store 5% of the produced hydrogen when $P_{wind} > P_{char}$ and will operate at the minimum load when $SOC < 1$, and store the surplus energy.

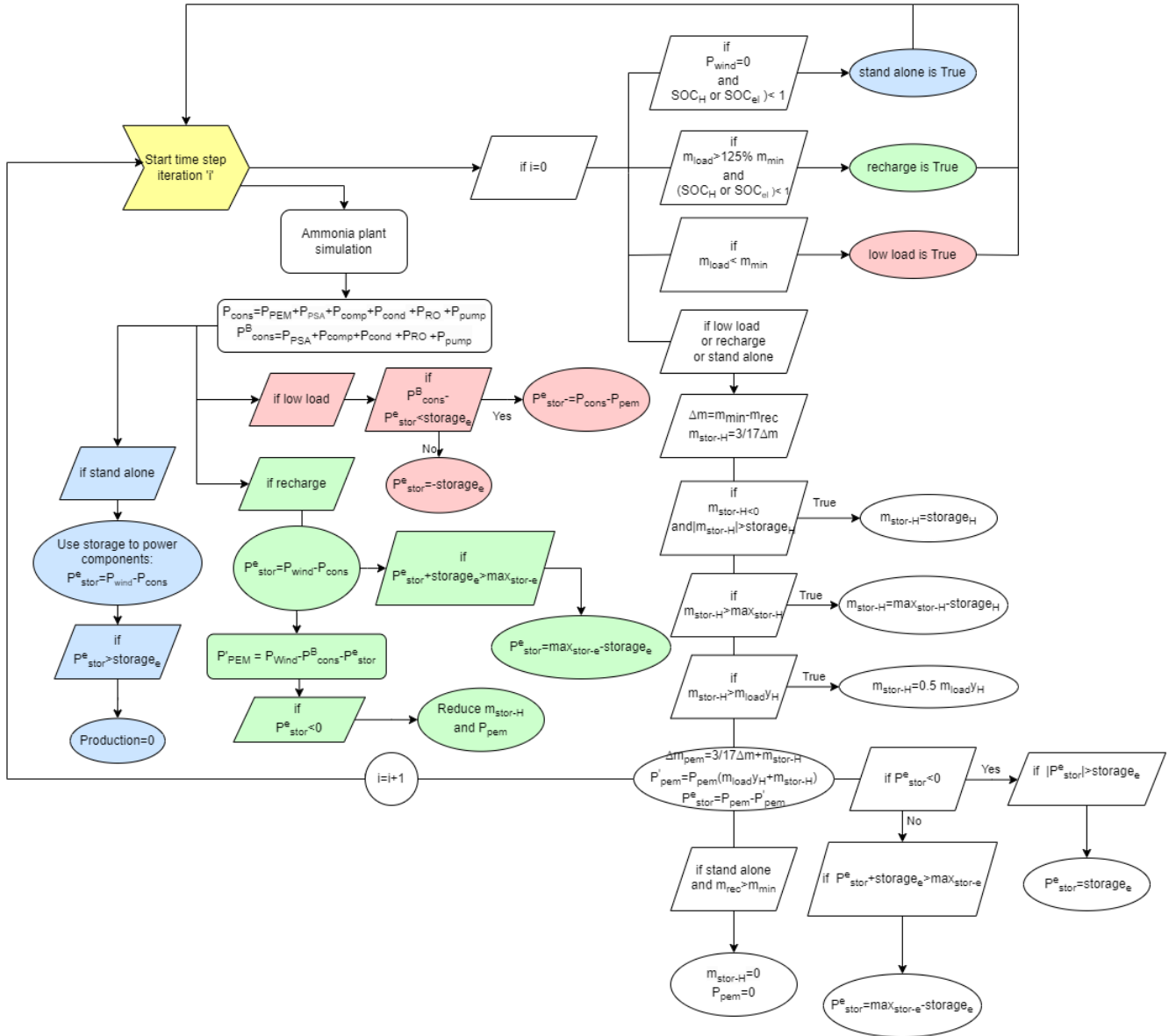


Figure 6.5: Storage code implementation.

In Figure 6.5 the control scheme for charging and discharging of the battery and the hydrogen tank is shown. Three different modes of operation are highlighted in blue, green, and red.

- *stand – alone*: highlighted in blue, aims to keep operation during the no production periods. The condition is met when the wind speed is below cut-in speed, see Section 4.1.1, therefore, $P_{wind} = 0$.
- *recharge*, in green, aims to recharge the electrical and hydrogen storage. This condition is met when the load is 5% over the minimum and the electrical or hydrogen storage is not fully charged.
- The *low – load* condition, in red, maintains operation over the minimum. The condition is met when the load is below minimum.

When *stand – alone* and *recharge* conditions are met, it is first verified whether the recycle stream is enough to operate the plant over the minimum as it has a significant contribution. During steady state operation the recycle stream account for around 70% of the total load in the plant 4.5. If this condition is verified the load is set equal to the recycle load. For the *stand – alone* case, this means that neither hydrogen nor nitrogen is produced, the electrical storage will be only used to sustain compression and cooling duties, for instance, the right part of Figure 3.3.

For the *recharge* the available electricity from the Pelton will be used to sustain the cycle, thus supplying energy for compression and cooling duties. All the hydrogen produced will recharge the hydrogen tank and the remaining electricity will recharge the battery.

When the recycle is not enough to allow operation over the minimum and one of the three conditions is verified, the plant is operated at the minimum load. This means that for *stand – alone* and *low – load*, the hydrogen necessary to satisfy the minimum load will be taken from the tank and is provided by Equation 6.3, while the electricity missing to operate the component at the minimum load will be supplied by the battery.

$$\Delta m = m_{min} - m_{load} \quad (6.2)$$

$$m_{stor}^h = \frac{3}{17} \Delta m \quad (6.3)$$

Δm is the amount of mass that has to be supplied(-), or that exceed the minimum load(+). m_{min} is the minimum load, m_{load} is the current load in the plant. m_{stor}^h is the hydrogen going to(+, charging)/coming from(-, discharging) the tank. $\frac{3}{17}$ is the weight ratio of the hydrogen-nitrogen mixture. Following the stoichiometric ratio, the feed mixture is composed of 3 moles of hydrogen and 1 of nitrogen, see Section 4.2.3, the molecular weight of hydrogen 2 kg/kmol and of nitrogen 28 kg/kmol, the result is that 3/17 of the mixture's weight is hydrogen.

For *recharge* the amount of hydrogen produced will be equal to the amount to reach the minimum load plus a quantity m_{stor}^h to recharge the tank in Equation 6.4.

$$m_{stor}^h = 0.75 \cdot \frac{3}{17} \Delta m \quad (6.4)$$

The hydrogen charging the tank m_{stor}^h is calculated as the one discharging the tank in Equation 6.3 but reduced by a factor 0.75. This reduction is necessary, to not only to store hydrogen but also electricity. By reducing the amount of hydrogen produced in the PEM, therefore, the energy requirements of the pem decrease and the surplus can be used to charge the battery.

The result of the above-mentioned conditions will be a flow of hydrogen m_{stor}^h from/to the storage (+ is charging, - if discharging), and a mass of hydrogen produced by the PEM, which corresponds a power P_{PEM} .

As described in Section 4 from the mass of hydrogen, the mass of nitrogen and the energy consumption for each component are known. This will allow to determine how much energy needs to be discharged from the battery:

$$P_{stor}^e = P_{wind} - P_{cons} \quad (6.5)$$

$$P_{cons} = P_{PEM} + P_{PSA} + P_{comp} + P_{comp}^{rec} + P_{cond} + P_{pump} + P_{RO} \quad (6.6)$$

Where P_{stor}^e is the flow of energy from/to the battery. P_{wind} is the power available from the wind, 0 in case of *standalone*. Note that if $P_{wind} < P_{cons}$, P_{stor}^e is negative and the battery is being discharged. P_{PEM} , P_{PSA} , P_{comp} , P_{comp}^{rec} , P_{cond} , P_{pump} and P_{RO} are respectively the power at the PEM, PSA, feed-compressors, recycle compressor, condenser and water pump (both for cooling duties and compressing the water).

Hydrogen will be stored at a pressure of 30 bar and 293 K [46]. The tank dimensions range from 50 kg to 100 kg. The different sizes are tested with the different minimum load changing from 20% to 50%.

6.5 Results with hydrogen storage

Result with a minimum load 50% of the nominal load are shown in Figure A.8 with the smallest hydrogen tank size, 50 kg, and in Figure A.9 with the biggest hydrogen tank size. None of the configurations is able to sustain such a minimum load when $P_{wind} = 0$. With such a minimum load an oversizing of the storage would be necessary.

The results show that it is necessary to reduce the minimum load. The plant is able to maintain continuous operation with a minimum load set to 20% and hydrogen tank of 100 kg, even when $P_{wind} = 0$. This result is presented in Figure 6.6. With this configuration, the battery and hydrogen minimum SOC are 0.1813 and 0.1735 respectively.

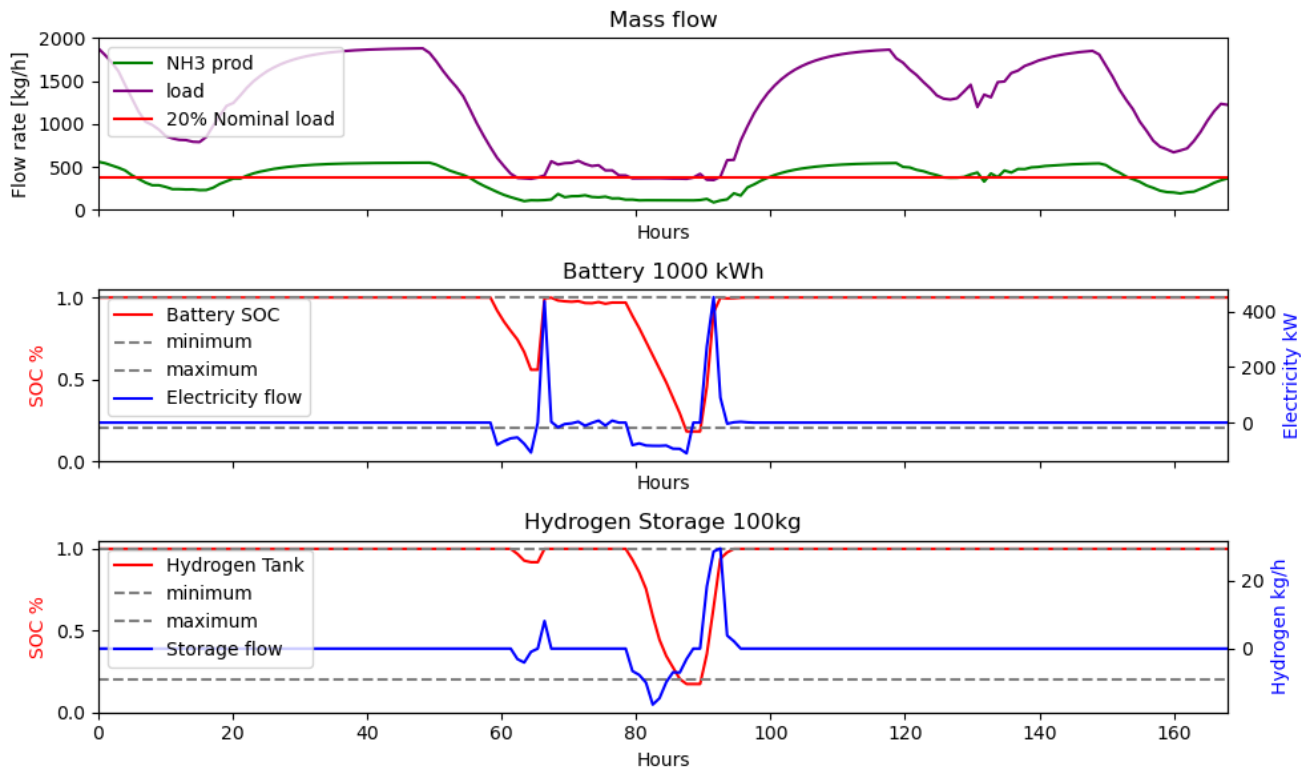


Figure 6.6: Results with a 100kg hydrogen tank and 20% minimum load. From top to bottom the total mass flow and ammonia produced in the plant, the battery, and the hydrogen tank.

Incorporating a hydrogen tank capable of meeting the hydrogen demand alleviates the need for the battery to accommodate the Proton Exchange Membrane (PEM) consumption. To optimize the utilization of the battery further, Figure 4.6 should be used as a reference. A decrease in pressure within the system could lead to additional reductions in energy consumption. Specifically, lowering the pressure ratio at the inlet of the electrolyzer could present an opportunity as this take up to 30% in Figure 4.6. This could be achieved with the HPP by regulating pressure at the outlet of the RO.

For this last configuration the ratio between ammonia energy and wind energy, per time step, is calculated as in Equation 5.1, but by considering also the storage:

$$\eta = \frac{m_{NH_3} e_{NH_3}}{E_{wind} - E_{storage}^{el} - E_{storage}^h - E_{storage}^{ro}} \quad (6.7)$$

Where m_{NH_3} is the mass of ammonia produced in the time step in kg, e is the energy density of ammonia in kJ/kg, and E_{wind} is the energy available from the wind in kJ, $E_{storage}^{el}$ the energy flow to/from the battery in kJ, $E_{storage}^h$ the energy corresponding to the hydrogen injected to/taken from the tank in kJ, $E_{storage}^{ro}$ the energy corresponding to the water flow to/from the tank in kJ.

The value is equal to 0.6845 at the rated condition, meaning that 68.45% of the energy harvested by the wind turbine is converted into ammonia. The value increases to a value higher than 1 when E_{wind} decreases. This is due to the beneficial effect of the recycle stream. A reduction in available E_{wind} causes a reduction of the feed gases, which accounts only for 30% of the total gases circulating in the plant 4.5, but which production takes up to 90% of the total energy consumption, as discussed in Section 4.5.

Given the significant influence of the recycle stream on the efficiency of ammonia production, it can serve as a crucial variable for designing an effective control strategy. Storage of the recycle stream could also be taken into consideration.

The capacity factor of the plant is calculated as in Equation 5.2. Due to the addition of storage, the capacity factor has increased to 0.6646 compared to the without storage simulation, indicating enhanced production continuity. By reducing the size of the plant and improving the control strategy for the storage, and higher capacity factor can be achieved.

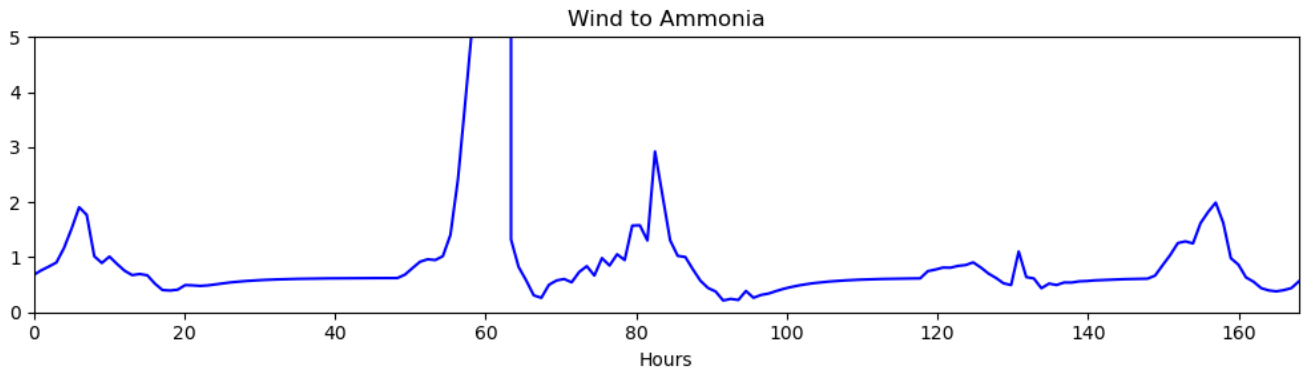


Figure 6.7: Wind to Ammonia. Energy obtained from produced ammonia over available wind energy per time step.

In Figure 6.8 the ammonia produced in yellow and the power harvested by the turbine in blue. The production of ammonia remains aligned with the available wind power, except during the period between time steps 60 and 100. During this interval, a storage system effectively maintains ammonia production almost constant, even in instances where wind power fluctuates down to zero.

The data presented in Figure 6.9 represents hydrogen production rates (kg/h) over the time period. Based on this data, it seems that the production rate fluctuates significantly.

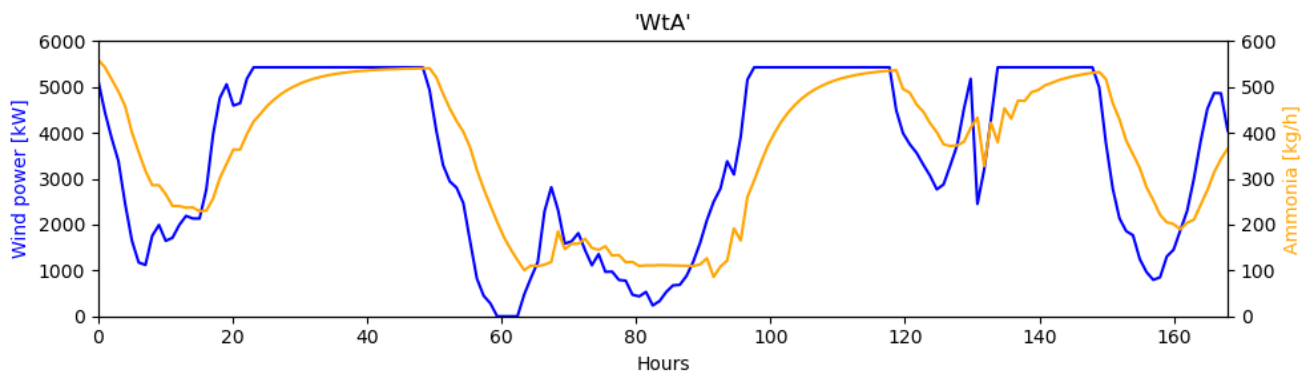


Figure 6.8: Ammonia produced and wind power per times step.

These fluctuations confirm the choice of PEM over AWE as the first one offer higher flexibility in terms of response to varying demand and potentially higher efficiency as already discussed in Section 3.4.

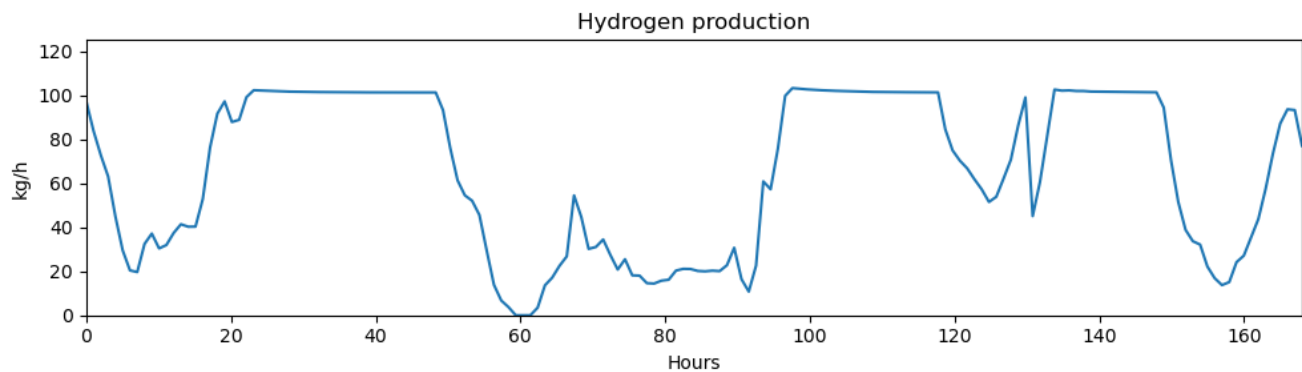


Figure 6.9: Hydrogen production over time.

Chapter 7

Conclusions and future outlooks

In conclusion, an ammonia plant powered by a **DOT** turbine would exhibit a well-integrated system starting from the wind turbine itself. Pressurized water, generated by the **HPP** located in the nacelle, is split between a Pelton turbine and **RO** unit for generating electricity and desalinated water, respectively. This desalinated water serves as the input for the electrolyzer, detailed in Section 3.4, while electricity is distributed among various energy-consuming components, including the electrolyzer, **ASU** using **PSA**, compressors, and condenser, as depicted in Figure 6.1. These technologies are characterized by a **TRL** exceeding 8, indicating their readiness for implementation within a system.

A wustite as **ZA-5** catalyst can be used to allow for milder, less energy-intensive, operative condition, such as 85 bar and 500-600 K.

Given the observed fluctuations in hydrogen production, a **PEM** electrolyzer is a preferable choice due to its higher flexibility and capability to handle dynamic operation.

From the simulation results, it was found that incorporating a storage system is essential to ensure continuous operation and prevent plant shutdowns. This system should include a water tank for storing desalinated water, a battery, and a hydrogen tank. While batteries are suitable for short-term energy storage, allowing for quick electrical load stabilization and balancing, they are not adequate for long-term storage. Hence, storing excess hydrogen in a tank is necessary to store excess hydrogen produced during periods of low demand, providing a reliable backup for sustaining operations during extended periods.

The Python model developed demonstrates a remarkable consistency with Aspen models used in the scientific literature for modelling large-scale ammonia production systems. The comparison indicates that typical large-scale systems achieve single-pass conversions of up to 26% and overall conversions between 97–99% with the inclusion of a recycle stream [46, 48]. In the model developed within this project, the global efficiency of the plant, defined as the ratio between input reactants and output ammonia, is calculated to be 94.46%, with individual conversion efficiencies of the first and second beds estimated at 25.99% and 17.67%, respectively. Furthermore, the fraction of the feed stream relative to the total mass rate circulating in the plant, at 30.92%, aligns with findings by Lin et al. [44] where the feed stream accounts for 25.54% of the total mass [?].

The total power consumption is determined to be 35.01 GJ/tonNH₃ or 9.86 kWh/kg, which closely resembles the values calculated by Cunanan et al. [46] (37.4 GJ per metric ton of ammonia) and Lin et al. [44] (9.70 kWh/kg NH₃). Additionally, the energy breakdown, particularly the dominance of the electrolyzer in energy consumption, echoes the findings of Lin et al. [44] and Cunanan et al. [46], where the electrolyzer accounts for 91.5% [44] and 88.07% [46] of the total energy consumption, respectively.

Overall, the Python model not only replicates the performance of large-scale ammonia production systems but also provides valuable insights into energy consumption patterns and efficiency. The model is divided in blocks, which can be easily accessed and modified, constituting a useful tool for further analysis and optimization.

Simulation results have demonstrated the storage system's potential to sustain operation even during periods of low or zero production. For the storage control strategy, a simple approach has been implemented to maintain a minimum load in the plant.

A preliminary sizing of the storage has been done, however for a proper design a longer wind period should be analyzed, storage and load profile should be optimized to overcome seasonal changes.

The efficiency, defined as the ratio between ammonia produced and wind energy available, has highlighted the crucial role of the recycle stream in buffering or dampening the overall load of the plant. Given that this stream constitutes a significant fraction of the load, any decrease in P_{wind} has a significant impact on hydrogen production. Results is that when power production is zero, the plant can continue operation by circulating the recycle stream, using around a tenth of the total energy consumption.

These findings suggest that the recycle stream could serve as a parameter for the control strategy of the interface between HBU and storage system,

A more sophisticated control strategy is required to ensure a more stable load. This strategy should be designed to regulate the operation of the storage system effectively, maintaining optimal performance and minimizing fluctuations in production.

Another finding from the simulation regards water production. The power allocated to the RO module is found to be minimal, below 3 kW with storage. In the configuration outlined in this project, it is determined that one DOT turbine out of 18 would suffice to supply the required amount of water, with an additional turbine included for redundancy. This observation suggests that approximately 10% of the turbines in a wind park could be dedicated to water production.

7.1 Future recommendations and limitations

Further research should consider a broader scope for the system integration, by including the modelling of the DOT turbine and of the RO. These comprises for the integration of both the turbine control strategy and the RO control strategy.

Regarding the RO control strategy, it's important to note that the DOT500 PRO system was initially designed for drinkable water production, primarily targeting remote islands or desert areas. The main focus has been on quickly establishing conditions for water production and maximizing water output. However, when the system is repurposed for ammonia production, the primary objective shifts towards maximizing electricity production. Therefore, careful consideration must be given to the design of the RO control strategy to align with the goal of electricity production for ammonia synthesis.

A more elaborated control strategy for the HB load and for water, electrical, and hydrogen storage, needs to be defined considering the dynamic nature of the plant, the minimum load, and the complex interplay between various components.

Future studies should consider utilizing 10-minute interval data for wind speed, instead of hourly data. Utilizing more frequent wind data allows for a more accurate representation of wind variability and patterns, which can significantly impact the performance and efficiency of wind-powered systems, and allows to analyze the battery's response in shorter timeframes.

Exploring the utilization of produced hydrogen or ammonia as fuel to power the plant presents another promising solution for ensuring continuous operation. The hydrogen or ammonia produced during ammonia synthesis can be stored and subsequently used as fuel in a fuel cell to produce electricity. This would make up for the battery as long-term electrical storage.

A more accurate definition of the plant performance can be obtained by including a more precise model for the electrolyzer, utilizing authentic electrolyzer datasheets. Given its substantial energy consumption, the electrolyzer's behavior holds significant relevance. Additionally, accounting for heat losses, particularly during lower load conditions, is crucial, as their influence on plant operations may be more pronounced.

Incorporating a hydrogen storage unit alongside the battery has the advantage of relieving the battery from directly supplying energy to the electrolyzer. By examining Figure 4.6, it becomes apparent how to enhance the battery's utilization. Increasing battery utilization can be achieved through various means, one of which involves lowering the system pressure, as demonstrated in innovative low-pressure ammonia production methods ([44]). Another approach involves optimizing the operation of the DOT turbine. Specifically, maintaining higher pressure in the permeate from the RO process to supply the electrolyzer can reduce the energy demand of the water pump, thereby enhancing overall energy efficiency and maximizing battery utilization. Further research can investigate in this direction.

Nomenclature

ΔH_R	Heat of reaction [$kJkmol^{-1}$]
ν_i	Stoichiometric coefficient
ϕ_i	Fugacity [-]
C_p	Specific heat capacity [$kJkmol^{-1}K^{-1}$]
E_a	Activation Energy [$kJkmol^{-1}$]
f_{purge}	Purge fraction [-]
k_0	Pre-exponential factor [$atm^{0.5}h^{-1}$]
K_f	Equilibrium constant [atm^{-1}]
k_T	Rate constant [$atm^{0.5}h^{-1}$]
u_i	Quenching fraction [-]
y_i	Fugacity coefficient [-]
m_{load}	Plant load [kg/h]
\dot{m}_{rated}	Plant rated load [kg/h]
$C_{p,mixture}$	Heat capacity of the mixture [kW]
E_{wind}	Wind energy [kJ]
F_i	Molar flow rate [$kmol s^{-1}$]
P'_{PEM}	PEM Power [kW]
$P_{storage}^h$	Hydrogen power storage [kJ]
P_{comp}	Feed in compressors power [kW]
P_{comp}^{rec}	Recycle compressor power [kW]
P_{cond}	Condenser power [kW]
P_{PEM}	PEM Power [kW]
P_{PSA}	PSA Power [kW]
P_{pump}	Water pump power [kW]
P_{RO}	RO power [kW]

$P_{storage}^{el}$ Flow of power to/from the battery [kW]

P_{wind} Wind power [kW]

Q_{cond} Heat removed by the condenser [kW]

Q_{cool} Heat removed by the cooler [kW]

r'_{NH_3} Rate of reaction [$kmolm^{-3}s^{-1}$]

V_{cat} Catalyst bed volume [m^3]

x_{H_2} Hydrogen weight fraction [-]

x_{N_2} Nitrogen weight fraction [-]

x_{NH_3} Ammonia weight fraction [-]

y_{H_2} Hydrogen molar fraction [-]

y_{N_2} Nitrogen molar fraction [-]

y_{NH_3} Ammonia molar fraction [-]

T Temperature [K]

Appendix A

A.1 Simulations results

In Figure A.1 the charging and discharging of a $10m^3$ water tank is shown. The tank discharges fully once over the period, showing that a bigger tank is necessary to decouple RO and Pelton usage.

In Figure A.1 the charging and discharging of a $20m^3$ water tank is shown. The minimum SOC is 0.47. It is worth noting that the tank is oversized for the considered period.

In Figure ?? the battery is charging and discharging. The battery charges only when $P_{wind} > P_{char}$.

In Figure A.5, A.6 and A.7 a 1000kW battery charging and discharging, with minimum load at 50%, 40% and 30% respectively. No hydrogen tank included.

In Figure A.8 hydrogen tank 50kg, minimum load at 50%. In Figure A.8 hydrogen tank 100kg, minimum load at 50%.

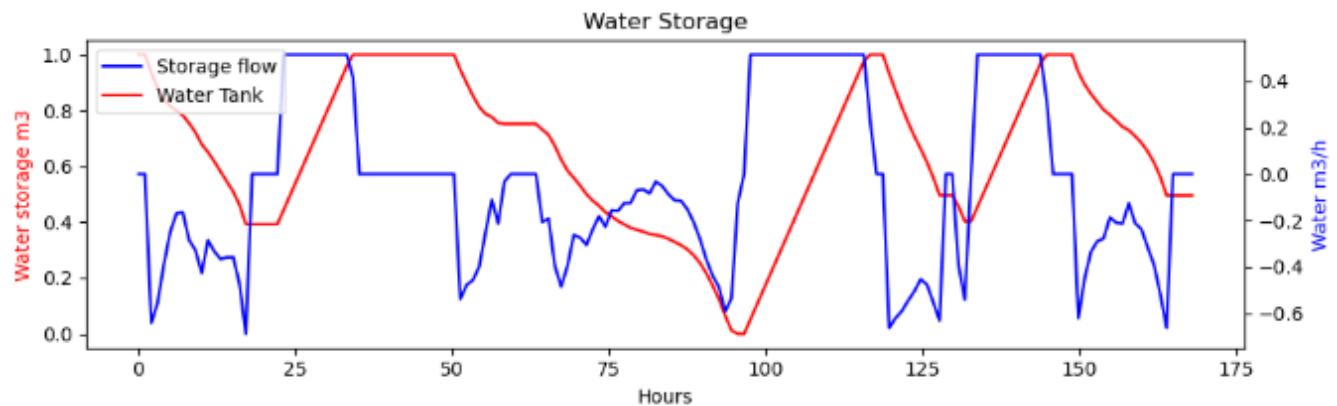


Figure A.1: Water tank charging/discharging, size $10m^3$.

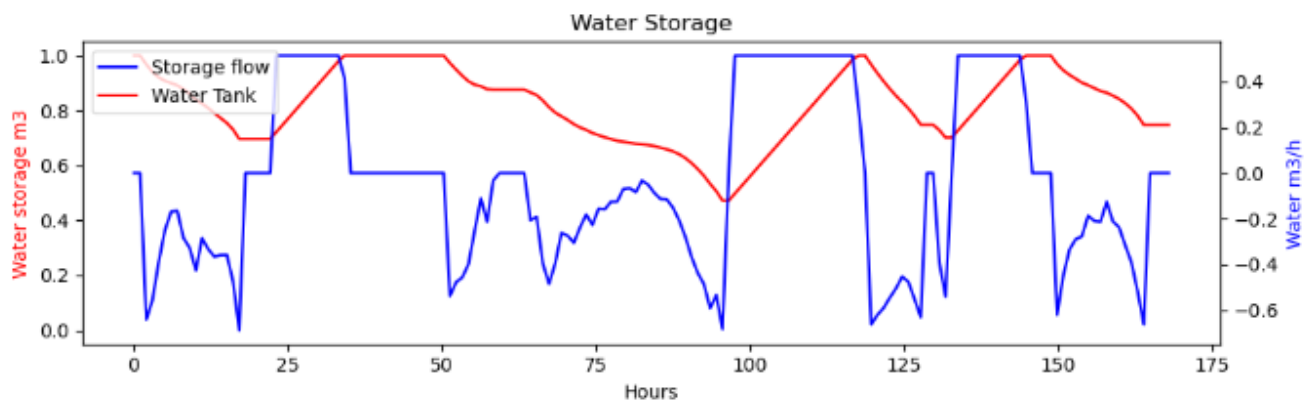


Figure A.2: Water tank charging/discharging, size $20m^3$.

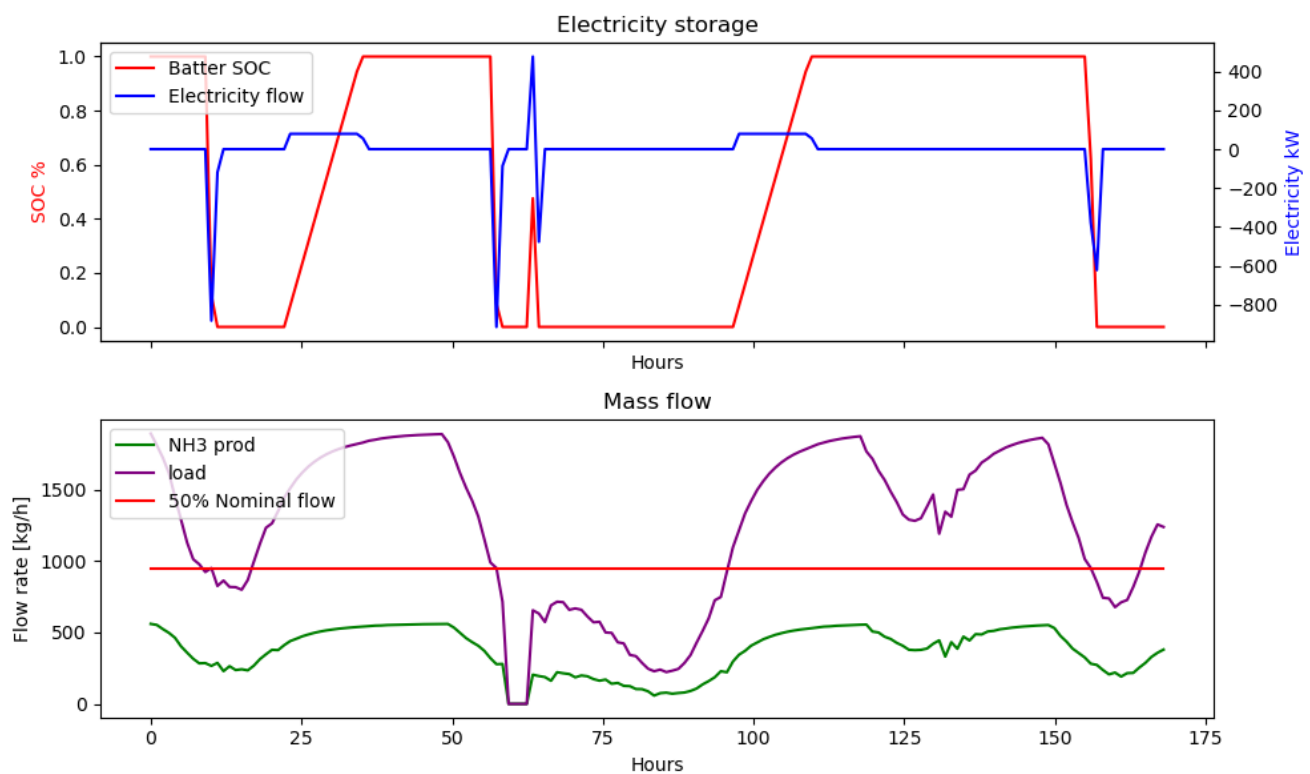


Figure A.3: On top battery SOC and charging/discharging power flow. On the bottom the load of the plant and the produced ammonia. The battery discharges when the load goes below 50% of the nominal load.

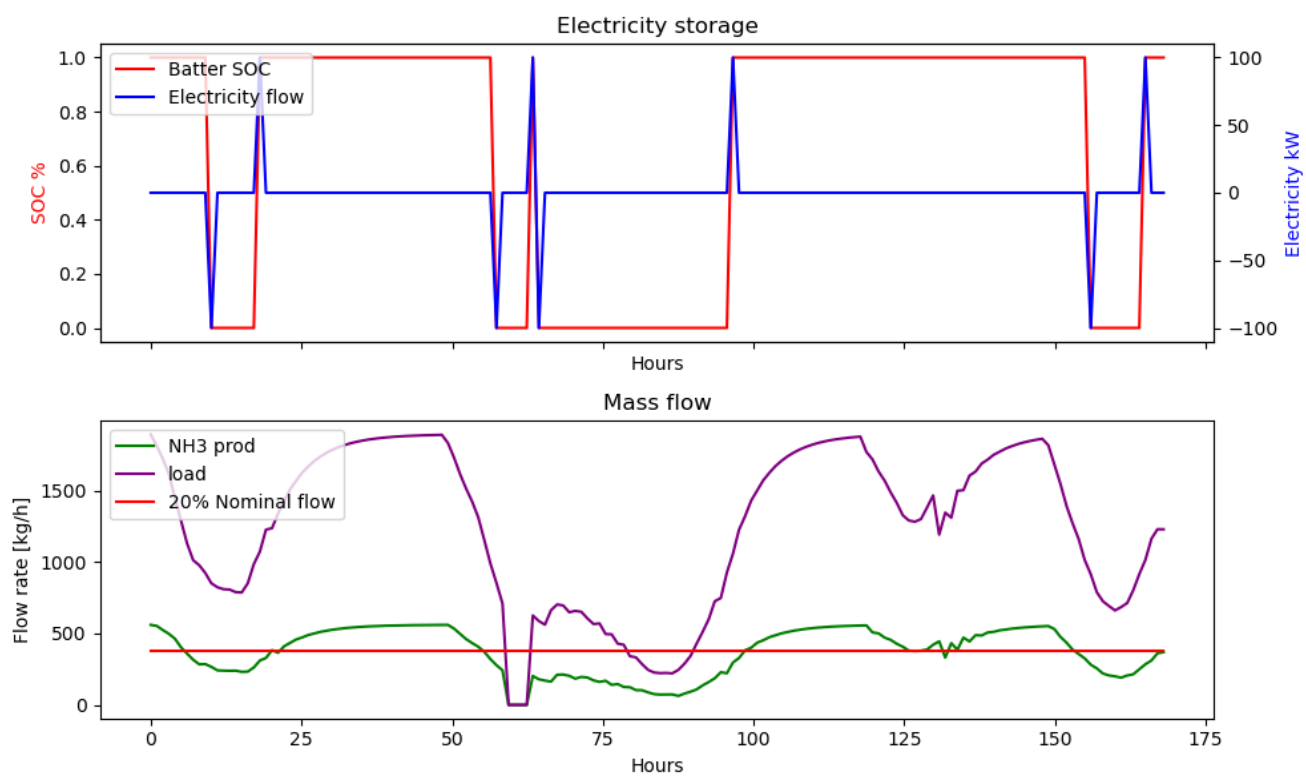


Figure A.4: On top battery charging/discharging. On the bottom the mass flow in the plant and the ammonia produced. The battery is 100kW and discharges when the load goes below 20%.

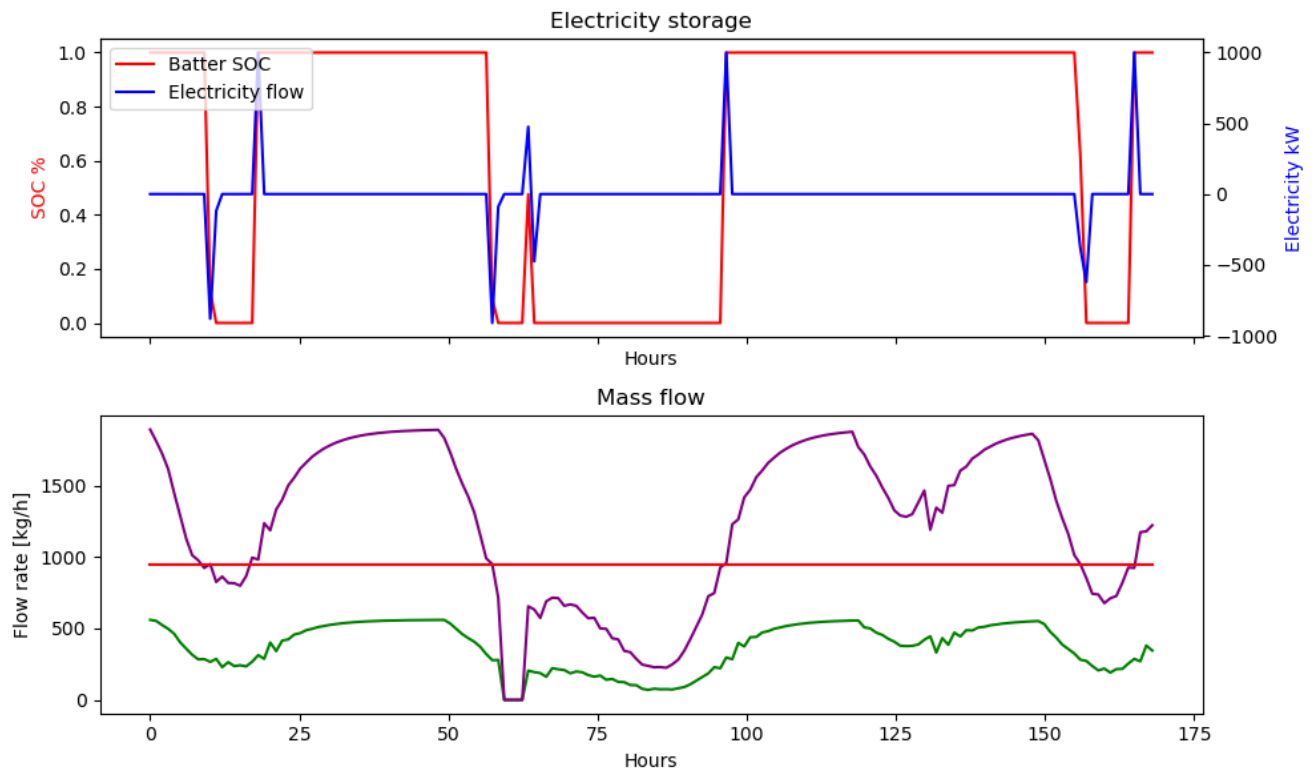


Figure A.5: On top battery charging/discharging. On the bottom the mass flow in the plant and the ammonia produced. The battery discharges when the load goes below 50%.

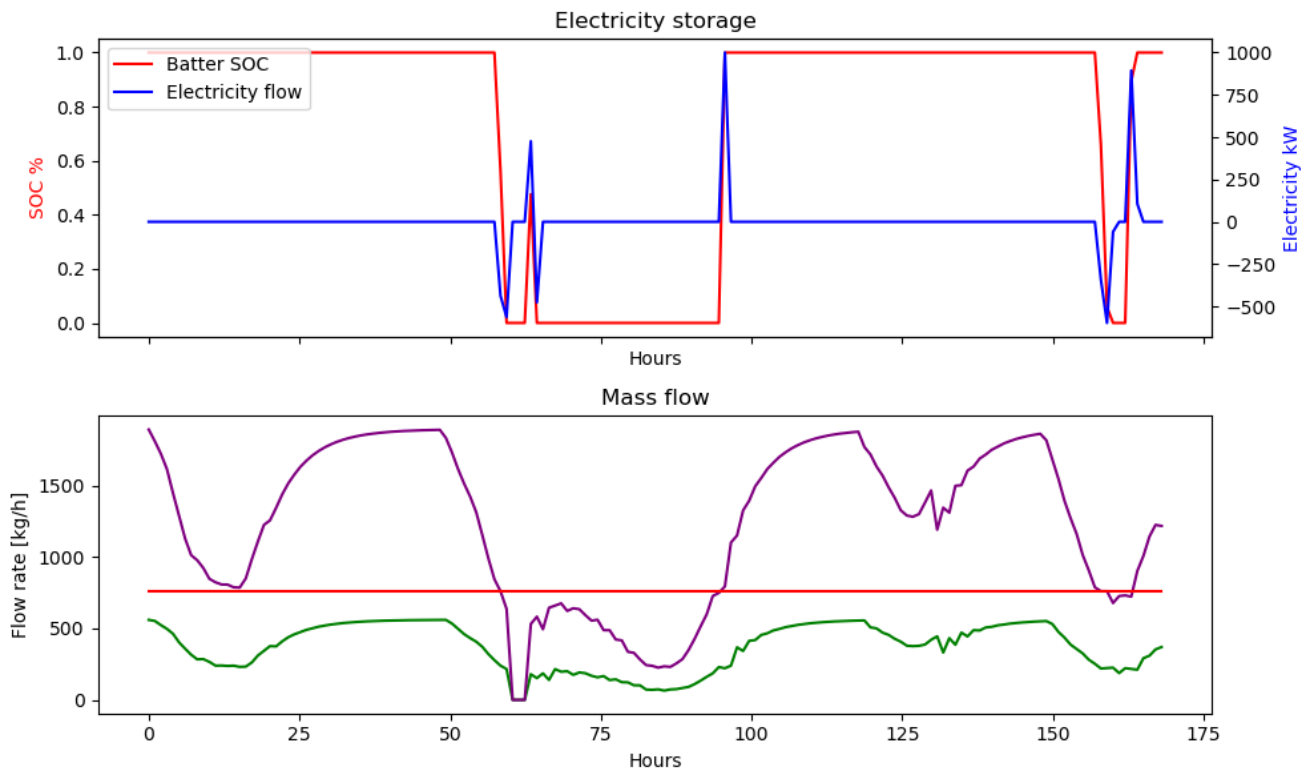


Figure A.6: On top battery charging/discharging. On the bottom the mass flow in the plant and the ammonia produced. The battery discharges when the load goes below 40%.

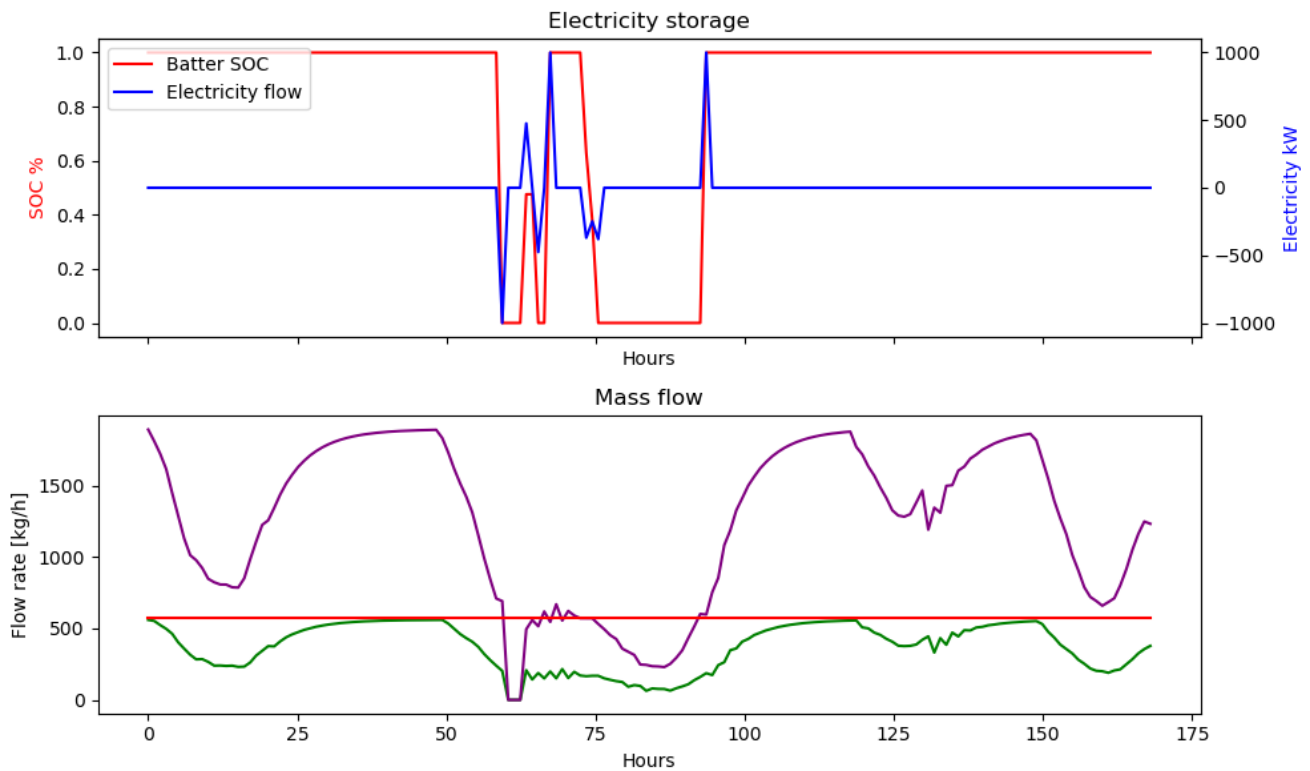


Figure A.7: On top battery charging/discharging. On the bottom the mass flow in the plant and the ammonia produced. The battery discharges when the load goes below 30%.

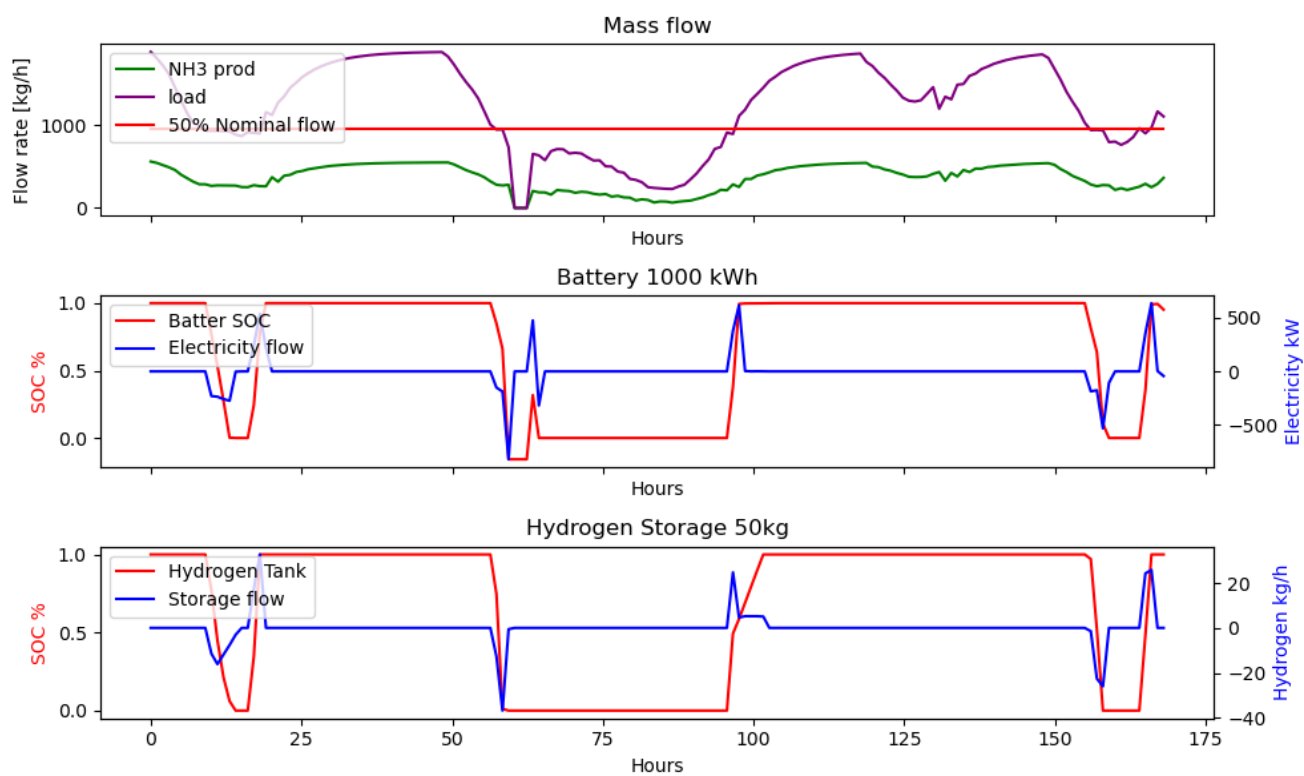


Figure A.8: Results with a 50kg hydrogen tank and 50% minimum load. From top to bottom the total mass flow and ammonia produced in the plant, the battery and the hydrogen tank.

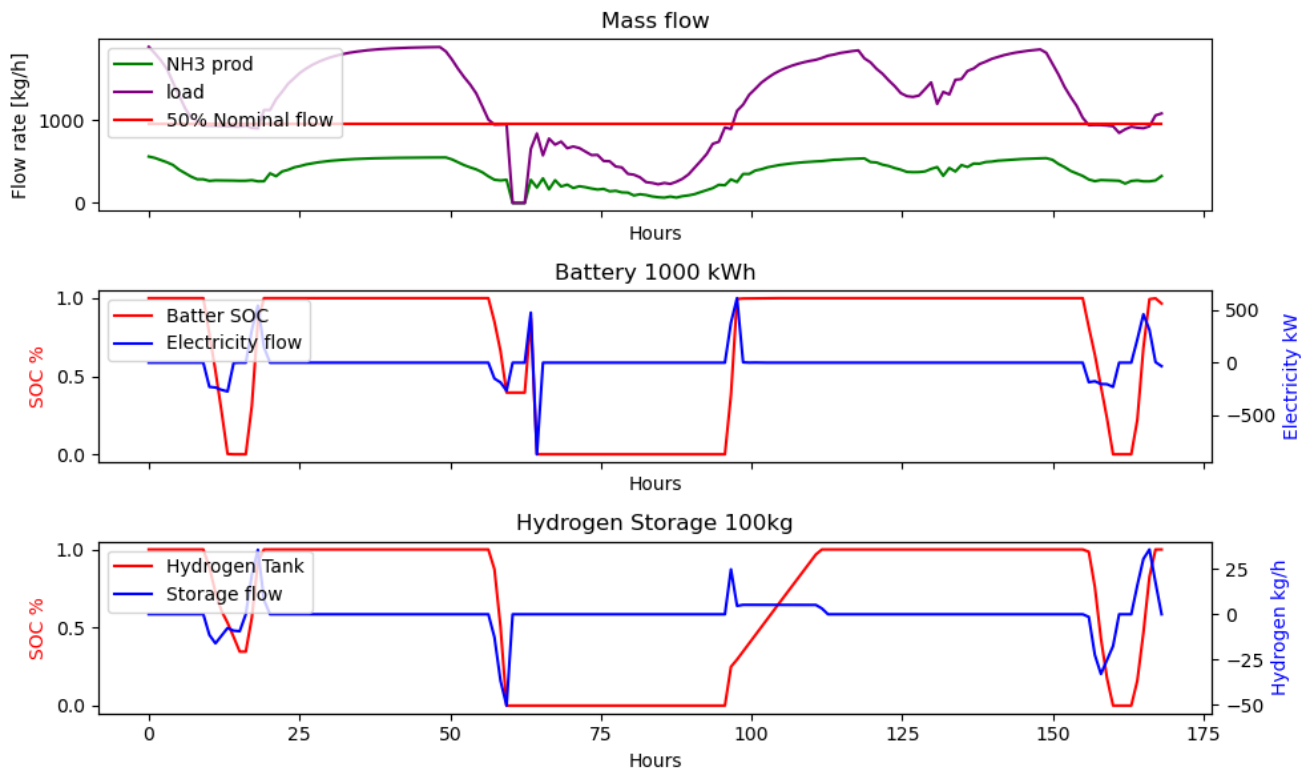


Figure A.9: Results with a 100kg hydrogen tank and 50% minimum load. From top to bottom the total mass flow and ammonia produced in the plant, the battery and the hydrogen tank.

Bibliography

- [1] Ammonia., n.d.. URL <https://en.wikipedia.org/wiki/Ammonia>.
- [2] Peter H Pfromm. Towards sustainable agriculture: Fossil-free ammonia. *Journal of Renewable and Sustainable Energy*, 9(3), 2017.
- [3] Wind turbine components, n.d. URL <https://windmillstech.com/wind-turbine-components/>.
- [4] Psa for your on-site high purity nitrogen generation., 2024. URL <https://medaad.com/psa-high-purity-nigtorgen-generation/>.
- [5] How reverse osmosis works, 2023-05-12. URL <https://science.howstuffworks.com/reverse-osmosis.htm>.
- [6] Kevin Hendrik Reindert Rouwenhorst, Piotr Marek Krzywda, Nieck E Benes, Guido Mul, and Leon Lefferts. Ammonia production technologies. *Techno-Economic Challenges of Green Ammonia as Energy Vector*, pages 41–84, 2020.
- [7] Climate change, n.d. URL <https://www.un.org/en/global-issues/climate-change>.
- [8] Climate change in data, 2024-02-01. URL <https://www.ipcc.ch/report/ar6/wg1/resources/climate-change-in-data/>.
- [9] United Nation. Climate action. URL <https://www.un.org/en/climatechange/science/causes-effects-climate-change>.
- [10] IRENA. Renewable power remains cost-competitive amid fossil fuel crisis. URL <https://www.irena.org/news/pressreleases/2022/Jul/Renewable-Power-Remains-Cost-Competitive-amid-Fossil-Fuel-Crisis>.
- [11] Duong Quoc Hung, Md Rakibuzzaman Shah, and Nadarajah Mithulananthan. Technical challenges, security and risk in grid integration of renewable energy. *Smart power systems and renewable energy system integration*, pages 99–118, 2016.
- [12] Kaveh Mazloomi and Chandima Gomes. Hydrogen as an energy carrier: Prospects and challenges. *Renewable and Sustainable Energy Reviews*, 16(5):3024–3033, 2012.
- [13] Lin Ye, Richard Nayak-Luke, Rene Banares-Alcantara, and Edman Tsang. Reaction: “green” ammonia production. *Chem*, 3(5):712–714, 2017.
- [14] Offshore wind: The netherlands well on schedule, tender round to double capacity will start early 2024, 2023-12-20. URL <https://www.government.nl/latest/news/2023/12/19/offshore-wind-the-netherlands-well-on-schedule-tender-round-to-double-capacity-will-start-early-2024>.
- [15] Keyi Liu, Wei Chen, Gexin Chen, Dandan Dai, Chao Ai, Xinwang Zhang, and Xin Wang. Application and analysis of hydraulic wind power generation technology. *Energy Strategy Reviews*, 48:101117, 2023.

- [16] Angeliki-Chrysoula Pytharoulou. Numerical simulation and operating strategy of a wind-powered electricity and freshwater production system, 2023.
- [17] History made by heerema with offshore testing campaign, 2024-03-01. URL <https://www.heerema.com/insights/history-made-by-heerema-with-offshore-testing-campaign>.
- [18] Gentle driving of piles (gdp), n.d. URL <https://grow-offshorewind.nl/project/gentle-driving-of-piles>.
- [19] Hydraulic pile extraction scale tests (hype-st), n.d. URL <https://grow-offshorewind.nl/project/hype-st>.
- [20] The role of hydrogen and ammonia in meeting the net zero challenge. *The Royal Society*, 2021. URL <https://royalsociety.org/-/media/policy/projects/climate-change-science-solutions/climate-science-solutions-hydrogen-ammonia.pdf>.
- [21] Grand view research, hydrogen generation market size, share and trends analysis report by system (merchant, captive), by technology (steam methane reforming, coal gasification), by application, by source, by region, and segment forecasts, 2023-2030. Technical report, Grand View Research, 2018-2022.
- [22] Seyedehhoma Ghavam, Maria Vahdati, IA Wilson, and Peter Styring. Sustainable ammonia production processes. *Frontiers in Energy Research*, 9:34, 2021.
- [23] Yanguang Zhao, Jing Hu, Lun Hua, Shijin Shuai, and Jianxin Wang. Ammonia storage and slip in a urea selective catalytic reduction catalyst under steady and transient conditions. *Industrial & engineering chemistry research*, 50(21):11863–11871, 2011.
- [24] Pragya Berwal, Sudarshan Kumar, and Bhupendra Khandelwal. A comprehensive review on synthesis, chemical kinetics, and practical application of ammonia as future fuel for combustion. *Journal of the Energy Institute*, 99:273–298, 2021.
- [25] How to feed the world in 2050? *FAO*, 2009.
- [26] Ammonia: Toxological review, n.d.. URL https://assets.publishing.service.gov.uk/media/5a81a887e5274a2e8ab552a6/Ammonia_TO_PHE_240815.pdf.
- [27] *The list of Extremely Hazardous Substances and Their Threshold Planning Quantities*, chapter Appendix A to 355. Government Printing Office.
- [28] Dindha Andriani and Yusuf Bicer. A review of hydrogen production from onboard ammonia decomposition: Maritime applications of concentrated solar energy and boil-off gas recovery. *Fuel*, 352: 128900, 2023.
- [29] Ammonia: Fuel vs. hydrogen carrier, 2024-03-01. URL <https://www.bv.com/perspectives/ammonia-fuel-vs-hydrogen-carrier/>.
- [30] João Sousa Cardoso, Valter Silva, Rodolfo C Rocha, Matthew J Hall, Mário Costa, and Daniela Eusébio. Ammonia as an energy vector: Current and future prospects for low-carbon fuel applications in internal combustion engines. *Journal of Cleaner Production*, 296:126562, 2021.
- [31] John Humphreys, Rong Lan, and Shanwen Tao. Development and recent progress on ammonia synthesis catalysts for haber–bosch process. *Advanced Energy and Sustainability Research*, 2(1): 2000043, 2021.

- [32] Rebecca Maria Brigitte Gullberg. Controllability analysis of ammonia synthesis loops. Master's thesis, NTNU, 2018.
- [33] Kevin Verleysen, Alessandro Parente, and Francesco Contino. How sensitive is a dynamic ammonia synthesis process? global sensitivity analysis of a dynamic haber-bosch process (for flexible seasonal energy storage). *Energy*, 232:121016, 2021.
- [34] Wind energy, n.d. URL <https://www.irena.org/Energy-Transition/Technology/Wind-energy>.
- [35] Parikshit G Jamdade, Santosh V Patil, and Shrinivas G Jamdade. Assessment of power coefficient of an offline wind turbine generator system. *Electronic Journal of Energy & Environment*, 1(3), 2013.
- [36] Tony Burton. *Wind Energy Handbook*. John Wiley and Sons, 2001.
- [37] Sandra Eriksson, Hans Bernhoff, and Mats Leijon. Evaluation of different turbine concepts for wind power. *renewable and sustainable energy reviews*, 12(5):1419–1434, 2008.
- [38] Kehinde Adeseye Adeyeye, Nelson Ijumba, and Jonathan Colton. The effect of the number of blades on the efficiency of a wind turbine. In *IOP Conference Series: Earth and Environmental Science*, volume 801, page 012020. IOP Publishing, 2021.
- [39] Deok-je Bang, Henk Polinder, G Shrestha, and Jan Abraham Ferreira. Review of generator systems for direct-drive wind turbines. In *European wind energy conference & exhibition, Belgium*, volume 31, pages 1–11, 2008.
- [40] Refuel, n.d. URL <https://arpa-e.energy.gov/technologies/programs/refuel>.
- [41] Michael Reese. Small scale ammonia synthesis using stranded wind energy, n.d. URL <https://wcroc.cfans.umn.edu/research/renewable-energy/ammonia-synthesis>.
- [42] Michael Reese. Ammonia production from wind energy gaining momentum, 2024-02-01. URL <https://wcroc.cfans.umn.edu/research/renewable-energy/ammonia-wind>.
- [43] Offshore ammonia production in greenland, January 17 2023. URL <https://www.ammoniaenergy.org/articles/offshore-ammonia-production-in-greenland/>.
- [44] Bosong Lin, Theodore Wiesner, and Mahdi Malmali. Performance of a small-scale haber process: A techno-economic analysis. *ACS Sustainable Chemistry & Engineering*, 8(41):15517–15531, 2020.
- [45] Izzat Iqbal Cheema and Ulrike Krewer. Operating envelope of haber–bosch process design for power-to-ammonia. *RSC advances*, 8(61):34926–34936, 2018.
- [46] Carlo James Cunanan, Carlos Andrés Elorza Casas, Mitchell Yorke, Michael Fowler, and Xiao-Yu Wu. Design and analysis of an offshore wind power to ammonia production system in nova scotia. *Energies*, 15(24):9558, 2022.
- [47] The haber process, n.d. URL <https://chemistrytalk.org/haber-process/>.
- [48] David E Brown, Terry Edmonds, Richard W Joyner, John J McCarroll, and Stephen R Tennison. The genesis and development of the commercial bp doubly promoted catalyst for ammonia synthesis. *Catalysis letters*, 144:545–552, 2014.
- [49] Kevin HR Rouwenhorst, Aloijsius GJ Van der Ham, and Leon Lefferts. Beyond haber-bosch: the renaissance of the claude process. *international journal of hydrogen energy*, 46(41):21566–21579, 2021.

- [50] Pierre Olivier, Cyril Bourasseau, and Pr Belkacem Bouamama. Low-temperature electrolysis system modelling: A review. *Renewable and Sustainable Energy Reviews*, 78:280–300, 2017.
- [51] MD Rashid, Mohammed K Al Mesfer, Hamid Naseem, and Mohd Danish. Hydrogen production by water electrolysis: a review of alkaline water electrolysis, pem water electrolysis and high temperature water electrolysis. *International Journal of Engineering and Advanced Technology*, 2015.
- [52] Ruxing Gao, Leiyu Zhang, Lei Wang, Xiudong Zhang, Chundong Zhang, Ki-Won Jun, Seok Ki Kim, Hae-Gu Park, Ying Gao, Yuezhao Zhu, et al. A comparative study on hybrid power-to-liquids/power-to-gas processes coupled with different water electrolysis technologies. *Energy Conversion and Management*, 263:115671, 2022.
- [53] Marcelo Carmo, David L Fritz, Jürgen Mergel, and Detlef Stolten. A comprehensive review on pem water electrolysis. *International journal of hydrogen energy*, 38(12):4901–4934, 2013.
- [54] D.S. Falcão and A.M.F.R. Pinto. A review on pem electrolyzer modelling: Guidelines for beginners. *Journal of Cleaner Production*, 261:121184, 2020. ISSN 0959-6526. doi: <https://doi.org/10.1016/j.jclepro.2020.121184>. URL <https://www.sciencedirect.com/science/article/pii/S0959652620312312>.
- [55] AR Smith and J Klosek. A review of air separation technologies and their integration with energy conversion processes. *Fuel processing technology*, 70(2):115–134, 2001.
- [56] Kevin H.R. Rouwenhorst, Aloijsius G.J. Van der Ham, Guido Mul, and Sascha R.A. Kersten. Islanded ammonia power systems: Technology review and conceptual process design. *Renewable and Sustainable Energy Reviews*, 114:109339, 2019. ISSN 1364-0321. doi: <https://doi.org/10.1016/j.rser.2019.109339>. URL <https://www.sciencedirect.com/science/article/pii/S1364032119305477>.
- [57] URL <https://www.noaa.gov/jetstream/atmosphere>.
- [58] F Greco, D De Bruycker, A Velez-Isaza, NFB Diepeveen, and A Jarquin-Laguna. Preliminary design of a hydraulic wind turbine drive train for integrated electricity production and seawater desalination. In *Journal of Physics: Conference Series*, volume 1618, page 032015. IOP Publishing, 2020.